CERN-TH/98-189
hep-ph/9806351

Measuring the Trilinear Couplings of MSSM Neutral Higgs Bosons at High-Energy e^+e^- Colliders

P. Osland[a,b,c] and P. N. Pandita[a,d]

[a] Department of Physics, University of Bergen, N-5007 Bergen, Norway*

[b] Deutsches Elektronen-Synchrotron DESY, D-22603 Hamburg, Germany

[c] Theoretical Physics Division, CERN, CH 1211 Geneva 23, Switzerland

[d] Department of Physics, North Eastern Hill University, Shillong 793 022, India*

Abstract

We present a detailed analysis of multiple production of the lightest CP-even Higgs boson (h) of the Minimal Supersymmetric Standard Model (MSSM) at high-energy e^+e^- colliders. We consider the production of the heavier CP-even Higgs boson (H) via Higgs-strahlung $e^+e^- \to ZH$, in association with the CP-odd Higgs boson (A) in $e^+e^- \to AH$, or via the fusion mechanism $e^+e^- \to \nu_e\bar{\nu}_e H$, with H subsequently decaying through $H \to hh$, thereby resulting in a pair of lighter Higgs bosons (h) in the final state. These processes can enable one to measure the trilinear Higgs couplings λ_{Hhh} and λ_{hhh}, which can be used to theoretically reconstruct the Higgs potential. We delineate the regions of the MSSM parameter space in which these trilinear Higgs couplings could be measured at a future e^+e^- collider. In our calculations, we include in detail the radiative corrections to the Higgs sector of the MSSM, especially the mixing in the squark sector.

PACS: 14.80.Cp, 12.60.Jv, 13.90.+i

---

* Permanent addresses

CERN-TH/98-189
June 1998

1 Introduction

The Higgs potential of the Standard Model (SM), which is crucial in implementing the mechanism of spontaneous symmetry breaking, contains the unknown quartic coupling of the Higgs field. As a consequence, the mass of the only Higgs boson in the SM, which is determined by this quartic coupling, is not known [1]. If a Higgs boson is discovered and its mass measured, the Higgs potential of the Standard Model can be uniquely determined.

On the other hand, supersymmetry is at present the only known framework in which the Higgs sector of the Standard Model (SM), so crucial for its internal consistency, is natural [2]. The minimal version of the Supersymmetric Standard Model (MSSM) contains two Higgs doublets (H_1, H_2) with opposite hypercharges: $Y(H_1) = -1$, $Y(H_2) = +1$, so as to generate masses for up- and down-type quarks (and leptons), and to cancel gauge anomalies. After spontaneous symmetry breaking induced by the neutral components of H_1 and H_2 obtaining vacuum expectation values, $\langle H_1 \rangle = v_1$, $\langle H_2 \rangle = v_2$, $\tan\beta = v_2/v_1$, the MSSM contains two neutral CP-even[1] (h, H), one neutral CP-odd (A), and two charged ($H^{\pm}$) Higgs bosons [1]. Although gauge invariance and supersymmetry fix the quartic couplings of the Higgs bosons in the MSSM in terms of $SU(2)_L$ and $U(1)_Y$ gauge couplings, g and g', respectively, there still remain two independent parameters that describe the Higgs sector of the MSSM. These are usually chosen to be $\tan\beta$ and m_A, the mass of the CP-odd Higgs boson. All the Higgs masses and the Higgs couplings in the MSSM can be described (at tree level) in terms of these two parameters.

In particular, all the trilinear self-couplings of the physical Higgs particles can be predicted theoretically (at the tree level) in terms of m_A and $\tan\beta$. Once a light Higgs boson is discovered, the measurement of these trilinear couplings can be used to reconstruct the Higgs potential of the MSSM. This will go a long way toward establishing the Higgs mechanism as the basic mechanism of spontaneous symmetry breaking in gauge theories. Although the measurement of all the Higgs couplings in the MSSM is a difficult task, preliminary theoretical investigations by Plehn, Spira and Zerwas [3], and by Djouadi,

[1] When unambiguous, we shall denote the CP-even Higgs particles as h and H.

Haber and Zerwas [4] (referred to as 'DHZ' in the following), of the measurement of these couplings at the LHC and at a high-energy e^+e^- linear collider, respectively, are encouraging.

In this paper we consider in detail the question of possible measurements of the trilinear Higgs couplings of the MSSM at a high-energy e^+e^- linear collider. We assume that such a facility will operate at an energy of 500 GeV with an integrated luminosity per year of $\mathcal{L}_{\rm int} = 500$ fb^{-1} [5]. (This is a factor of 10 more than the earlier estimate.) In a later phase one may envisage an upgrade to an energy of 1.5 TeV. Since the 'interesting' cross sections fall off like $1/E^2$, the luminosity should increase by a corresponding factor. An earlier estimated luminosity of 500 fb^{-1} at 1.5 TeV may turn out to be too conservative.

The trilinear Higgs couplings that are of interest are λ_{Hhh}, λ_{hhh}, and λ_{hAA}, involving both the CP-even (h, H) and CP-odd (A) Higgs bosons.[2] The couplings λ_{Hhh} and λ_{hhh} are rather small with respect to the corresponding trilinear coupling $\lambda^{\rm SM}_{hhh}$ in the SM (for a given mass of the lightest Higgs boson m_h), unless m_h is close to the upper value (decoupling limit). The coupling λ_{hAA} remains small for all parameters.

Throughout, we include one-loop radiative corrections [6] to the Higgs sector in the effective potential approximation. In particular, we take into account the parameters A and μ, the soft supersymmetry breaking trilinear parameter and the bilinear Higgs(ino) parameter in the superpotential, respectively, and as a consequence the left–right mixing in the squark sector, in our calculations. We thus include all the relevant parameters of the MSSM in our study, which is more detailed than the preliminary one of DHZ.

For a given value of m_h, the values of these couplings significantly depend on the soft supersymmetry-breaking trilinear parameter A, as well as on μ, and thus on the resulting mixing in the squark sector. Since the trilinear couplings tend to be small, and depend on several parameters, their effects are somewhat difficult to estimate.

The plan of the paper is as follows. In Section 2 we review the Higgs sector of the

[2]These are not the only couplings that occur in the Higgs potential. However, these are the only ones which could possibly be measured at future colliders.

MSSM, including the radiative corrections to the masses. The trilinear couplings are presented in Section 3. In Section 4 we review the possible production mechanisms for the multiple production of Higgs bosons through which the trilinear Higgs couplings can be measured at an e^+e^- linear collider. In Section 5 we consider the dominant source of the multiple production of the Higgs (h) boson through Higgs-strahlung of H, and through production of H in association with the CP-odd Higgs boson (A), and the background to these processes. This source of multiple production can be used to extract the trilinear Higgs coupling λ_{Hhh}.

Section 6 deals with a detailed calculation of the cross section for the double Higgs-strahlung process $e^+e^- \to Zhh$. This process involves the trilinear couplings λ_{Hhh} and λ_{hhh} of the CP-even Higgs bosons (h, H). In Section 7 we consider the different fusion mechanisms for multiple h production, especially the non-resonant process $e^+e^- \to \nu_e\bar{\nu}_e hh$, for which we present a detailed calculation of the cross section in the 'effective WW approximation'. This process also involves the two trilinear Higgs couplings, λ_{Hhh} and λ_{hhh}, and is the most useful one for extracting the coupling λ_{hhh}. In Section 8 we present, based on our calculations, the regions of the MSSM parameter space in which the trilinear couplings λ_{Hhh} and λ_{hhh} could be measured; finally, in Section 9 we present a summary of our results and conclusions.

2 The Higgs Sector of the MSSM

In this section we review the Higgs sector of the Minimal Supersymmetric Standard Model in order to set the notation and to describe the approximations we use in our calculations. As mentioned in the introduction, we shall include the dependence on the parameters A and μ through mixing in the squark sector. Where there is an overlap, our notation and approach closely follow those of Ref. [4].

At the tree level, the Higgs sector of the MSSM is described by two parameters, which can be conveniently chosen as m_A and $\tan\beta$ [1]. There are, however, substantial radiative corrections to the CP-even neutral Higgs masses and couplings [6]. In the one-

loop effective potential approximation, the radiatively corrected squared-mass matrix for the CP-even Higgs bosons can be written as [7]

$$\begin{aligned}\mathcal{M}^2 &= \begin{bmatrix} m_A^2 \sin^2\beta + m_Z^2 \cos^2\beta & -(m_Z^2 + m_A^2)\sin\beta\cos\beta \\ -(m_Z^2 + m_A^2)\sin\beta\cos\beta & m_A^2\cos^2\beta + m_Z^2\sin^2\beta \end{bmatrix} \\ &\quad + \frac{3g^2}{16\pi^2 m_W^2}\begin{bmatrix} \Delta_{11} & \Delta_{12} \\ \Delta_{12} & \Delta_{22} \end{bmatrix}, \end{aligned} \tag{2.1}$$

where the second matrix represents the radiative corrections.[3]

The functions Δ_{ij} depend, besides the top- and bottom-quark masses, on the Higgs bilinear parameter μ in the superpotential, the soft supersymmetry-breaking trilinear couplings (A_t, A_b) and soft scalar masses (m_Q, m_U, m_D), as well as on $\tan\beta$. We shall ignore the b-quark mass effects in Δ_{ij} in our calculations, which is a reasonable approximation for moderate values of $\tan\beta \lesssim 20$–30. Furthermore, we shall assume, as is often done,

$$\begin{aligned} A &\equiv A_t = A_b, \\ \tilde{m} &\equiv m_Q = m_U = m_D. \end{aligned} \tag{2.2}$$

With these approximations we can write (m_t is the top quark mass) [7]:

$$\Delta_{11} = \frac{m_t^4}{\sin^2\beta}\left(\frac{\mu(A+\mu\cot\beta)}{m_{\tilde{t}_1}^2 - m_{\tilde{t}_2}^2}\right)^2 g(m_{\tilde{t}_1}^2, m_{\tilde{t}_2}^2), \tag{2.3}$$

$$\begin{aligned}\Delta_{22} &= \frac{m_t^4}{\sin^2\beta}\left(\log\frac{m_{\tilde{t}_1}^2 m_{\tilde{t}_2}^2}{m_t^4} + \frac{2A(A+\mu\cot\beta)}{m_{\tilde{t}_1}^2 - m_{\tilde{t}_2}^2}\log\frac{m_{\tilde{t}_1}^2}{m_{\tilde{t}_2}^2}\right) \\ &\quad + \frac{m_t^4}{\sin^2\beta}\left(\frac{\mu(A+\mu\cot\beta)}{m_{\tilde{t}_1}^2 - m_{\tilde{t}_2}^2}\right)^2 g(m_{\tilde{t}_1}^2, m_{\tilde{t}_2}^2), \end{aligned} \tag{2.4}$$

$$\Delta_{12} = \frac{m_t^4}{\sin^2\beta}\frac{\mu(A+\mu\cot\beta)}{m_{\tilde{t}_1}^2 - m_{\tilde{t}_2}^2}\left(\log\frac{m_{\tilde{t}_1}^2}{m_{\tilde{t}_2}^2} + \frac{A(A+\mu\cot\beta)}{m_{\tilde{t}_1}^2 - m_{\tilde{t}_2}^2} g(m_{\tilde{t}_1}^2, m_{\tilde{t}_2}^2)\right), \tag{2.5}$$

[3] We note that two-loop corrections to the Higgs masses in the MSSM are sizable, especially for large mixing in the stop sector. For the dominant two-loop radiative corrections to the Higgs sector of the MSSM, see, e.g. [8]. In this paper we restrict ourselves to one-loop corrections only.

where $m^2_{\tilde{t}_1}$ and $m^2_{\tilde{t}_2}$ are squared stop masses given by

$$m^2_{\tilde{t}_{1,2}} = m_t^2 + \tilde{m}^2 \pm m_t(A + \mu \cot\beta) \tag{2.6}$$

(we have ignored the small D-term contributions to the stop masses) and

$$g(m^2_{\tilde{t}_1}, m^2_{\tilde{t}_2}) = 2 - \frac{m^2_{\tilde{t}_1} + m^2_{\tilde{t}_2}}{m^2_{\tilde{t}_1} - m^2_{\tilde{t}_2}} \log \frac{m^2_{\tilde{t}_1}}{m^2_{\tilde{t}_2}}. \tag{2.7}$$

The one-loop radiatively corrected masses (m_h, m_H; $m_h < m_H$) of the CP-even Higgs bosons (h, H) can be obtained by diagonalizing the 2×2 mass matrix in Eq. (2.1). The radiative corrections are, in general, positive, and they shift the mass of the lightest Higgs boson upwards from its tree-level value. We show in Fig. 1 the resulting mass of the lightest Higgs boson, m_h, as a function of μ and $\tan\beta$, for two values of A and two values of m_A, and for $\tilde{m} = 1$ TeV. With a wider range of parameter values, or when the squark mass scale is taken to be smaller, the dependence on μ and $\tan\beta$ can be more dramatic [9].

The Higgs mass falls rapidly at small values of $\tan\beta$. Since the LEP experiments are obtaining lower bounds on the mass of the lightest Higgs boson, they are beginning to rule out significant parts of the small-$\tan\beta$ parameter space, depending on the model assumptions. For $\tan\beta > 1$, ALEPH finds $m_h > 62.5$ GeV at 95% C.L. [10].[4] In our calculations, we shall therefore take $\tan\beta = 2$ to be a representative value. [For a recent discussion on how the lower allowed value of $\tan\beta$ depends on some of the model parameters, see Ref. [12].]

[4]Recently, a new study has been presented, with a lower limit of $m_h > 72.2$ GeV, irrespective of $\tan\beta$, and a limit of ~ 88 GeV for $1 < \tan\beta \lesssim 2$ [11].

3 Trilinear Higgs couplings

The trilinear Higgs couplings that are of interest can be written [13] as a sum of the tree-level coupling and one-loop radiative corrections:

$$\lambda_{Hhh} = \lambda^0_{Hhh} + \Delta\lambda_{Hhh}, \tag{3.1}$$

$$\lambda_{hhh} = \lambda^0_{hhh} + \Delta\lambda_{hhh}, \tag{3.2}$$

$$\lambda_{hAA} = \lambda^0_{hAA} + \Delta\lambda_{hAA}. \tag{3.3}$$

In units of $gm_Z/(2\cos\theta_{\rm W}) = (\sqrt{2}G_F)^{1/2}m_Z^2$, the tree-level couplings are given by

$$\lambda^0_{Hhh} = 2\sin 2\alpha\sin(\beta+\alpha) - \cos 2\alpha\cos(\beta+\alpha), \tag{3.4}$$

$$\lambda^0_{hhh} = 3\cos 2\alpha\sin(\beta+\alpha), \tag{3.5}$$

$$\lambda^0_{hAA} = \cos 2\beta\sin(\beta+\alpha), \tag{3.6}$$

with α the mixing angle in the CP-even Higgs sector, which can be calculated in terms of the parameters appearing in the CP-even Higgs mass matrix (2.1). The one-loop radiative corrections in (3.1)–(3.3) are (in the above units):

$$\begin{aligned}
\Delta\lambda_{Hhh} &= \left(\frac{3g^2\cos^2\theta_W}{16\pi^2}\frac{m_t^4}{m_W^4}\frac{\sin\alpha\cos^2\alpha}{\sin^3\beta}\right) \\
&\times \left[3\log\frac{m^2_{\tilde t_1}m^2_{\tilde t_2}}{m_t^4} + (m^2_{\tilde t_1}-m^2_{\tilde t_2})C_t(E_t+2F_t)\log\frac{m^2_{\tilde t_1}}{m^2_{\tilde t_2}}\right. \\
&\quad +2\left(\frac{m_t^2}{m^2_{\tilde t_1}}\left[1+(m^2_{\tilde t_1}-m^2_{\tilde t_2})C_tE_t\right]\left[1+(m^2_{\tilde t_1}-m^2_{\tilde t_2})C_tF_t\right]^2\right. \\
&\quad \left.\left. + \frac{m_t^2}{m^2_{\tilde t_2}}\left[1-(m^2_{\tilde t_1}-m^2_{\tilde t_2})C_tE_t\right]\left[1-(m^2_{\tilde t_1}-m^2_{\tilde t_2})C_tF_t\right]^2 - 2\right)\right],
\end{aligned} \tag{3.7}$$

$$\begin{aligned}
\Delta\lambda_{hhh} &= \left(\frac{3g^2\cos^2\theta_W}{16\pi^2}\frac{m_t^4}{m_W^4}\frac{\cos^3\alpha}{\sin^3\beta}\right) \\
&\times \left[3\log\frac{m^2_{\tilde t_1}m^2_{\tilde t_2}}{m_t^4} + 3(m^2_{\tilde t_1}-m^2_{\tilde t_2})C_tF_t\log\frac{m^2_{\tilde t_1}}{m^2_{\tilde t_2}}\right. \\
&\quad \left. + 2\left(\frac{m_t^2}{m^2_{\tilde t_1}}\left[1+(m^2_{\tilde t_1}-m^2_{\tilde t_2})C_tF_t\right]^3 + \frac{m_t^2}{m^2_{\tilde t_2}}\left[1-(m^2_{\tilde t_1}-m^2_{\tilde t_2})C_tF_t\right]^3 - 2\right)\right],
\end{aligned} \tag{3.8}$$

$$
\begin{aligned}
\Delta\lambda_{hAA} &= \left(\frac{3g^2\cos^2\theta_W}{16\pi^2}\frac{m_t^4}{m_W^4}\frac{\cos\alpha\cos^2\beta}{\sin^3\beta}\right) \\
&\times \left[\log\frac{m_{\tilde{t}_1}^2 m_{\tilde{t}_2}^2}{m_t^4} + (m_{\tilde{t}_1}^2 - m_{\tilde{t}_2}^2)(D_t^2 + C_t F_t)\log\frac{m_{\tilde{t}_1}^2}{m_{\tilde{t}_2}^2}\right. \\
&\left. + (m_{\tilde{t}_1}^2 - m_{\tilde{t}_2}^2)^2 C_t D_t^2 F_t\, g(m_{\tilde{t}_1}^2, m_{\tilde{t}_2}^2)\right], \qquad (3.9)
\end{aligned}
$$

where

$$
\begin{aligned}
C_t &= (A + \mu\cot\beta)/(m_{\tilde{t}_1}^2 - m_{\tilde{t}_2}^2), \\
D_t &= (A - \mu\tan\beta)/(m_{\tilde{t}_1}^2 - m_{\tilde{t}_2}^2), \\
E_t &= (A + \mu\cot\alpha)/(m_{\tilde{t}_1}^2 - m_{\tilde{t}_2}^2), \\
F_t &= (A - \mu\tan\alpha)/(m_{\tilde{t}_1}^2 - m_{\tilde{t}_2}^2), \qquad (3.10)
\end{aligned}
$$

and we have ignored the contributions from b-quarks and b-squarks, which are in general small with respect to those arising from t-quarks and t-squarks. We have also adopted the simplification described in Eq. (2.2) in writing the above results. We shall make these approximations throughout this paper.

We show in Figs. 2, 3 and 4 the couplings λ_{Hhh}, λ_{hhh} and λ_{hAA} as functions of μ and $\tan\beta$, for two values of A and two values of m_A, all for $\tilde{m} = 1$ TeV. The explicit dependence on A and μ is not dramatic, but it should be kept in mind that unless m_A is rather small, m_h may change considerably with A.

The trilinear couplings change significantly with m_A, and thus also with m_h. This is shown more explicitly in Fig. 5, where we compare λ_{Hhh}, λ_{hhh} and λ_{hAA} for three different values of $\tan\beta$, and the SM quartic coupling $\lambda^{\rm SM}$. The SM quartic coupling includes one-loop radiative corrections [14], and its normalization is such that at the tree-level, it coincides with the trilinear coupling.

At low values of m_h, the MSSM trilinear couplings are rather small. For some value of m_h the couplings λ_{Hhh} and λ_{hhh} start to increase in magnitude, whereas λ_{hAA} remains small. The values of m_h at which they start becoming significant depend crucially on $\tan\beta$. For $\tan\beta = 2$ (Fig. 5a) this transition takes place around $m_h \sim$ 90–100 GeV, whereas for $\tan\beta = 5$ and 15, the critical values of m_h increase to 100–110 and 120 GeV,

respectively (see Figs. 5b and c). In this region, the actual values of λ_{Hhh} and λ_{hhh} (for a given value of m_h) change significantly if A becomes large and positive. A non-vanishing squark-mixing parameter A is thus seen to be quite important. Also, we note that for special values of the parameters, the couplings may vanish [15]. See also Fig. 1 of Ref. [3].

To sum up the behaviour of the trilinear couplings, we note that λ_{Hhh} and λ_{hhh} are small (≤ 1) for $m_h \lesssim$ 100–120 GeV, depending on the value of $\tan\beta$. However, as m_h approaches its maximum value, which is reached rapidly as m_A becomes large, $m_A \gtrsim 200$ GeV, these trilinear couplings become large ($\sim 2-4$). Thus, as functions of m_A, the trilinear couplings λ_{Hhh} and λ_{hhh} are large for most of the parameter space. We also note that, for large values of $\tan\beta$, λ_{Hhh} tends to be relatively small, whereas λ_{hhh} becomes large, if also m_A (or, equivalently, m_h) is large.

We note that for a given Higgs boson mass m_h, the tree level SM trilinear Higgs coupling is given by

$$\lambda_{hhh}^{\rm SM} = 3(m_h/m_Z)^2. \tag{3.11}$$

On the other hand, for large values of m_A (the decoupling limit) the corresponding MSSM trilinear coupling, Eq. (3.5), becomes

$$\lambda_{hhh}^{0} = 3\cos(2\alpha)\sin(\beta+\alpha) \to 3(m_h/m_Z)^2, \tag{3.12}$$

i.e., it approaches the SM trilinear coupling.

4 Production mechanisms

The different mechanisms for the multiple production of the MSSM Higgs bosons in e^+e^- collisions have been discussed by DHZ. The dominant mechanism for the production of multiple CP-even light Higgs bosons (h) is through the production of the heavy CP-even Higgs boson H, which then decays by $H \to hh$. The heavy Higgs boson H can be produced by H-strahlung, in association with A, and by the resonant WW fusion

mechanism. These mechanisms for multiple production of h

$$\left.\begin{array}{rcl} e^+e^- & \to & ZH, AH \\ e^+e^- & \to & \nu_e\bar{\nu}_e H \end{array}\right\}, \qquad H \to hh, \tag{4.1}$$

are shown in Fig. 6. We note that all the diagrams of Fig. 6 involve the trilinear coupling λ_{Hhh}.

A background to (4.1) comes from the production of the pseudoscalar A in association with h and its subsequent decay to hZ

$$e^+e^- \to hA, \qquad A \to hZ, \tag{4.2}$$

leading to Zhh final states [see Fig. 7d].

A second mechanism for hh production is double Higgs-strahlung in the continuum with a Z boson in the final state [see Fig. 7a–d],

$$e^+e^- \to Z^* \to Zhh. \tag{4.3}$$

We note that the Feynman diagram of Fig. 7c involves, apart from the coupling λ_{Hhh}, the trilinear Higgs coupling λ_{hhh} as well, whereas the other diagrams do not involve any of the trilinear Higgs couplings.

A third way of generating multiple Higgs bosons in e^+e^- collisions is through associated production of (hh) with the pseudoscalar A in the continuum [see Fig. 8]:

$$e^+e^- \to Z^* \to hhA. \tag{4.4}$$

This process will be briefly discussed in Section 6. It involves, besides λ_{Hhh} and λ_{hhh}, the trilinear coupling λ_{hAA} as well. It is, however, difficult [4] to measure this coupling λ_{hAA} through the process (4.4).

Finally, there is a mechanism of multiple production of the lightest Higgs boson through non-resonant WW (ZZ) fusion in the continuum [see Fig. 9]:

$$e^+e^- \to \bar{\nu}_e\nu_e W^*W^* \to \bar{\nu}_e\nu_e hh, \tag{4.5}$$

which will be discussed in Section 7.

It is important to note that all the diagrams of Fig. 6 involve the trilinear coupling λ_{Hhh} only. On the other hand, Fig. 7c, Fig. 8b and Fig. 9c all involve both the trilinear Higgs couplings λ_{Hhh} and λ_{hhh}.

5 Higgs-strahlung and Associated Production of H

As stated in Section 4, the dominant source for the production of multiple Higgs bosons (h) in e^+e^- collisions is through the production of the heavier CP-even Higgs boson H either via Higgs-strahlung or in association with A [1], followed, if kinematically allowed, by the cascade decay $H \to hh$. In terms of the Z-electron couplings $v_e = -1 + 4\sin^2\theta_W$, $a_e = -1$, the cross sections for these processes can be written as [16, 17]

$$\sigma(e^+e^- \to ZH) = \frac{G_F^2 m_Z^4}{96\pi s}(v_e^2 + a_e^2)\cos^2(\beta-\alpha)\frac{\lambda_Z^{1/2}\left[\lambda_Z + 12m_Z^2/s\right]}{(1-m_Z^2/s)^2}, \tag{5.1}$$

$$\sigma(e^+e^- \to AH) = \frac{G_F^2 m_Z^4}{96\pi s}(v_e^2 + a_e^2)\sin^2(\beta-\alpha)\frac{\lambda_A^{3/2}}{(1-m_Z^2/s)^2}, \tag{5.2}$$

where λ_j refers to $\lambda(m_j^2, m_H^2; s)$, the two-body phase-space function, and is given as

$$\lambda(m_a^2, m_b^2; m_c^2) = \left(1 - \frac{m_a^2}{m_c^2} - \frac{m_b^2}{m_c^2}\right)^2 - \frac{4m_a^2 m_b^2}{m_c^4}. \tag{5.3}$$

In Fig. 10 we plot the cross sections (5.1) and (5.2) for the e^+e^- centre-of-mass energies $\sqrt{s} = 500$ GeV and 1.5 TeV, as functions of the Higgs mass m_H and for $\tan\beta = 2.0$. For large values of the mass m_A of the pseudoscalar Higgs boson, all the Higgs bosons, except the lightest one (h), become heavy and decouple [18] from the rest of the spectrum. In this case

$$\cos^2(\beta-\alpha) \simeq \frac{m_Z^4 \sin^2 4\beta}{4m_A^4}, \tag{5.4}$$

and the associated AH production (5.2) becomes the dominant production mechanism for H.

At values of $\tan\beta$ that are not too large, the trilinear Hhh coupling λ_{Hhh} can be measured by the decay process $H \to hh$, which has a width

$$\Gamma(H \to hh) = \frac{G_F \lambda_{Hhh}^2}{16\pi\sqrt{2}}\frac{m_Z^4}{m_H}\left(1 - \frac{4m_h^2}{m_H^2}\right)^{1/2}. \tag{5.5}$$

However, this is possible only if the decay is kinematically allowed, and the branching ratio is sizeable. In Fig. 11 we show the branching ratios (at $\tan\beta = 2$) for the main decay modes of the heavy CP-even Higgs boson as a function of the H mass. Apart from the hh decay mode, the other important decay modes are $H \to WW^*$, ZZ^*. (We have here disregarded decays to supersymmetric particles: charginos, stops, etc. If such particles are kinematically accessible, the $H \to hh$ and $A \to Zh$ rates could be much smaller [19].) We note that the couplings of H to gauge bosons can be measured through the production cross sections for $e^+e^- \to \nu_e\bar{\nu}_e H$; therefore the branching ratio $BR(H \to hh)$ can be used to measure the triple Higgs coupling λ_{Hhh}.

The Higgs-strahlung process [Fig. 6a, Eq. (5.1)] gives rise to resonant two-Higgs [hh] final states. This is to be contrasted with the associated production process [Fig. 6b, Eq. (5.2)], which typically yields three Higgs $h[hh]$ final states, since the channel $A \to hZ$ is the dominant decay mode of A in the mass range of interest. The decay width for $A \to hZ$ can be written as [20]

$$\Gamma(A \to hZ) = \frac{G_F}{8\pi\sqrt{2}} \cos^2(\beta-\alpha) \frac{m_Z^4}{m_A} \lambda^{1/2}(m_Z^2, m_h^2; m_A^2) \lambda(m_A^2, m_h^2; m_Z^2), \tag{5.6}$$

where the λ are phase-space factors given by Eq. (5.3). In Fig. 11 we show the branching ratios for the pseudoscalar A for $\tan\beta = 2.0$.

A background to the multiple production of lighter Higgs bosons h comes from hh states generated in the sequential reaction $e^+e^- \to Ah \to [Zh]h$ [see Fig. 7d]. This is a genuine background in the sense that no Higgs self-couplings are involved. But these background events are expected to be topologically very different from the signal events, since the two h bosons do not form a resonance, whereas the $[Zh]$ does. The cross section for the process $e^+e^- \to Ah$ can be written as [17]

$$\sigma(e^+e^- \to Ah) = \frac{G_F^2 m_Z^4}{96\pi s}(v_e^2 + a_e^2) \cos^2(\beta-\alpha) \frac{\lambda^{3/2}(m_h^2, m_A^2; s)}{(1 - m_Z^2/s)^2}, \tag{5.7}$$

and is shown in Fig. 10 together with the signal cross sections (5.1) and (5.2). As a consequence of the decoupling theorem [18], the cross section becomes small for large values of m_H.

For increasing values of $\tan\beta$, the Hhh coupling gradually gets weaker (see Figs. 2 and 5), and hence the prospects for measuring λ_{Hhh} diminish. This is indicated by Fig. 12, where we show the H and A branching ratios for $\tan\beta = 5$.

There is in fact a sizeable region in the m_A–$\tan\beta$ plane where the decay $H \to hh$ is kinematically forbidden. This is indicated in Fig. 13. In this figure we also display the regions where the $H \to hh$ branching ratio is in the range 0.1–0.9. Clearly, in the forbidden region, the λ_{Hhh} cannot be determined from resonant production.

6 Double Higgs-strahlung and Triple h Production

For small and moderate values of $\tan\beta$, the study of decays of the heavy CP-even Higgs boson H provides a means of determining the triple-Higgs coupling λ_{Hhh}. In order to extract the coupling λ_{hhh}, other processes involving two-Higgs (h) final states must be considered. The Zhh final states, which can be produced in the double Higgs-strahlung $e^+e^- \to Zhh$ of Fig. 7, could provide one possible opportunity, since it involves the coupling λ_{hhh} through the mechanism of Fig. 7c. In this section we shall study these non-resonant processes in detail.

6.1 The Double Higgs-strahlung $e^+e^- \to Zhh$

The doubly differential cross section for the process $e^+e^- \to Zhh$ shown in Fig. 7 can be written as [4]

$$\frac{d\sigma(e^+e^- \to Zhh)}{dx_1 dx_2} = \frac{G_F^3 m_Z^6}{384\sqrt{2}\pi^3 s}(v_e^2 + a_e^2)\frac{\mathcal{A}}{(1-\mu_Z)^2}, \tag{6.1}$$

where the couplings v_e and a_e have been defined at the beginning of Section 5. Because of some misprints in the formulas given in [4] for the coefficient $\mathcal{A}$, we have recalculated it. Following [4], we introduce $x_{1,2} = 2E_{1,2}/\sqrt{s}$ for the scaled energies of the Higgs particles, $x_3 = 2 - x_1 - x_2$ for the scaled energy of the Z boson, and $y_k = 1 - x_k$. Also, we denote by $\mu_i = m_i^2/s$ the scaled squared masses of various particles:

$$\mu_h = m_h^2/s, \qquad \mu_H = m_H^2/s, \qquad \mu_W = m_W^2/s. \tag{6.2}$$

We can express our result in a compact form as follows:

$$\mathcal{A} = \mu_Z \left\{ \tfrac{1}{2}|a|^2 f_a + |b(y_1)|^2 f_b + 2\,\mathrm{Re}[ab^*(y_1)]\, g_{ab} + \mathrm{Re}[b(y_1)b^*(y_2)]\, g_{bb} \right\} + \{x_1 \leftrightarrow x_2\}. \tag{6.3}$$

Here,

$$a = \frac{1}{2}\left[\frac{\sin(\beta-\alpha)\lambda_{hhh}}{y_3+\mu_Z-\tilde{\mu}_h} + \frac{\cos(\beta-\alpha)\lambda_{Hhh}}{y_3+\mu_Z-\tilde{\mu}_H}\right] + \left[\frac{\sin^2(\beta-\alpha)}{y_1+\mu_h-\tilde{\mu}_Z} + \frac{\sin^2(\beta-\alpha)}{y_2+\mu_h-\tilde{\mu}_Z}\right] + \frac{1}{2\mu_Z} \tag{6.4}$$

represents a contribution from diagram 7a, where the lepton tensor couples directly to the final-state Z polarization tensor, as well as the contributions of diagrams 7b and 7c. Similarly,

$$b(y) = \frac{1}{2\mu_Z}\left(\frac{\sin^2(\beta-\alpha)}{y+\mu_h-\tilde{\mu}_Z} + \frac{\cos^2(\beta-\alpha)}{y+\mu_h-\tilde{\mu}_A}\right) \tag{6.5}$$

represents the part of diagram 7a where the lepton tensor couples to the final-state Z polarization tensor indirectly via the Higgs momenta q_1 and q_2, as well as diagram 7d. The tildes on μ_i keep track of the widths, e.g. $\tilde{\mu}_Z = (m_Z^2 + i m_Z \Gamma_Z)/s$.

The Higgs self-couplings λ_{Hhh} and λ_{hhh} occur only in the function a, Eq. (6.4). The coefficients f and g, which do not involve any Higgs couplings, can be expressed rather compactly as

$$\begin{aligned}
f_a &= x_3^2 + 8\mu_Z, \\
f_b &= (x_1^2 - 4\mu_h)[(y_1-\mu_Z)^2 - 4\mu_Z\mu_h], \\
g_{ab} &= \mu_Z[2(\mu_Z - 4\mu_h) + x_1^2 + x_2(x_2+x_3)] - y_1(2y_2 - x_1x_3), \\
g_{bb} &= \mu_Z^2(4\mu_h + 6 - x_1x_2) + 2\mu_Z(\mu_Z^2 + y_3 - 4\mu_h) \\
&\quad + (y_3 - x_1x_2 - x_3\mu_Z - 4\mu_h\mu_Z)(2y_3 - x_1x_2 - 4\mu_h + 4\mu_Z).
\end{aligned} \tag{6.6}$$

These coefficients (we use a mixed notation, which involves both x and y) correspond to those of [4] as follows: $(f_a, f_b, g_{ab}, g_{bb}) = (f_0, f_1, f_3, f_2)$. With this identification, we agree with the result given in the Erratum to [4].

In the limit of large m_A, $\sin(\beta-\alpha) \to 1$, the cross section reduces to the Standard Model cross section with

$$a = \frac{1}{2}\frac{\lambda_{hhh}}{y_3+\mu_Z-\tilde{\mu}_h} + \left[\frac{1}{y_1+\mu_h-\tilde{\mu}_Z}+\frac{1}{y_2+\mu_h-\tilde{\mu}_Z}\right]+\frac{1}{2\mu_Z} \tag{6.7}$$

$$b(y) = \frac{1}{2\mu_Z}\frac{1}{y+\mu_h-\tilde{\mu}_Z}, \tag{6.8}$$

where at the tree level, $\lambda_{hhh} \to \lambda_{hhh}^{\rm SM}$, as discussed in Sec. 3.

We show in Fig. 14a the Zhh cross section, as given by Eqs. (5.1), (5.5) and (6.1), in the limit of no squark mixing, and with $\tilde{m} = 1$ TeV. The structure around $m_h = 70$ GeV is due to the vanishing and near-vanishing of the trilinear coupling. In Fig. 14b–d we have introduced squark mixing: $A = 1$ TeV, $\mu = 0, \pm 1$ TeV. (For the decoupling-limit cross section, which is also shown, we use the MSSM coupling, instead of the SM coupling, for the reason given in Sec. 3.)

In the case of no mixing, there is a broad minimum from $m_h \simeq 78$ to 90 GeV, followed by an enhancement around $m_h \sim 90$–100 GeV. This structure is due to the vanishing of the branching ratio for $H \to hh$, which is kinematically forbidden in the region $m_h \simeq 78$–90 GeV, see Fig. 13 (this coincides with the opening up of the channel $H \to WW$), followed by an increase of the trilinear couplings. This particular structure depends considerably on the exact mass values m_H and m_h. Thus, it depends on details of the radiative corrections and the mixing parameters A and μ.

The $A \to hZ$ channel contributes of the order of 20% in the region of the maximum at $m_h = 90$–100 GeV.

6.2 Triple-h production

The resonant and non-resonant production of Ahh [Fig. 8] can lead to three-h final states in the region of m_A, where A has a significant branching ratio for decaying to Zh, i.e. for m_A below the $t\bar{t}$ threshold, and relatively low values of $\tan\beta$ [cf. Figs. 11 and 12].

In principle, this channel allows for a study of the coupling λ_{hAA} [cf. Fig. 8a]. However, the prospects for measuring this coupling, which is rather small [see Fig. 4], was studied in Ref. [4] and found not to be very encouraging.

7 Fusion Mechanism for Multiple-h Production

As mentioned in Section 4, a double Higgs (hh) final state in e^+e^- collisions can also result from the WW fusion mechanism, which can either be a resonant process as in (4.1), or a non-resonant one like (4.5). Since the neutral-current couplings are smaller than the charged-current ones, the cross section for the ZZ fusion mechanism in (4.1) and (4.5) is an order of magnitude smaller than the WW fusion mechanism. We shall thus, in the following, ignore the ZZ fusion mechanism, and concentrate instead on the WW mechanism.

7.1 Resonant WW fusion

The WW fusion mechanism provides another large cross section for the multiple production of h bosons. The cross section for $e^+e^- \to H\bar{\nu}_e\nu_e$ can be written as [21]

$$\sigma(e^+e^- \to H\bar{\nu}_e\nu_e) = \frac{G_F^3 m_W^4}{64\sqrt{2}\pi^3}\left[\int_{\mu_H}^1 dx \int_x^1 \frac{dy}{\left[1+(y-x)/\mu_W\right]^2}\,\mathcal{F}(x,y)\right]\cos^2(\beta-\alpha), \quad (7.1)$$

where

$$\begin{aligned}
\mathcal{F}(x,y) &= 16[F(x,y)+G(x,y)], && (7.2)\\
F(x,y) &= \left[\frac{2x}{y^3}-\frac{1+2x}{y^2}+\frac{2+x}{2y}-\frac{1}{2}\right]\left[\frac{z}{1+z}-\log(1+z)\right]+\frac{x}{y^3}\frac{z^2(1-y)}{(1+z)}, && (7.3)\\
G(x,y) &= \left[-\frac{x}{y^2}+\frac{2+x}{2y}-\frac{1}{2}\right]\left[\frac{z}{1+z}-\log(1+z)\right], && (7.4)
\end{aligned}$$

with μ_i defined by Eq. (6.2) and

$$z = \frac{y(x-\mu_H)}{\mu_W x}. \quad (7.5)$$

For $\sqrt{s}$, $m_H \gg m_W$, and in the effective longitudinal W approximation, the cross section (7.1) for $e^+e^- \to H\bar{\nu}_e\nu_e$ can be written in the following simple form [22]

$$\sigma(e^+e^- \to H\bar{\nu}_e\nu_e) = \frac{G_F^3 m_W^4}{4\sqrt{2}\,\pi^3}\left[\left(1+\frac{m_H^2}{s}\right)\log\frac{s}{m_H^2}-2\left(1-\frac{m_H^2}{s}\right)\right]\cos^2(\beta-\alpha). \quad (7.6)$$

However, in this approximation the cross section may be overestimated by a factor of 2 for small values of masses and/or small centre-of-mass energies. For example, at $\sqrt{s} =$

500 GeV the equivalent W approximation gives a result that is twice as large as the exact cross section. Therefore, we use the exact cross section (7.1) in our calculations.

The cross section (7.1) is plotted in Fig. 10 for centre-of-mass energies, $\sqrt{s} = 500$ GeV and 1.5 TeV, and for $\tan\beta = 2.0$, as a function of m_H. The resonant fusion mechanism, which leads to $[hh]$ + [missing energy] final states is competitive with the process $e^+e^- \to HZ \to [hh]$ + [missing energy], particularly at high energies. Since the dominant decay of h will be into $b\bar{b}$ pairs, the H-strahlung and the fusion mechanism will give rise to final states that will predominantly include four b-quarks. On the other hand, the process $e^+e^- \to AH$ will give rise to six b-quarks in the final state, since the AH final state typically yields three-Higgs $h[hh]$ final states.

7.2 Non-resonant fusion $WW \to hh$

Besides the resonant WW fusion mechanism for the multiple production of h bosons, there is also a non-resonant WW fusion mechanism:

$$e^+e^- \to \nu_e\bar{\nu}_e hh, \tag{7.7}$$

through which the same final state of two h bosons can be produced. The cross section for this process, which arises through WW exchange as indicated in Fig. 9, can be written in the 'effective WW approximation' as[5]

$$\sigma(e^+e^- \to \nu_e\bar{\nu}_e hh) = \int_\tau^1 \mathrm{d}x\, \frac{\mathrm{d}L}{\mathrm{d}x}\, \hat{\sigma}_{WW}(x), \tag{7.8}$$

where $\tau = 4m_h^2/s$. In the above, the cross section is written as a WW cross section, at invariant energy squared $\hat{s} = xs$, folded with the WW 'luminosity' [22]:

$$\frac{\mathrm{d}L(x)}{\mathrm{d}x} = \frac{G_\mathrm{F}^2 m_W^4}{2} \left(\frac{v^2+a^2}{4\pi^2}\right)^2 \frac{1}{x}\left\{(1+x)\log\frac{1}{x} - 2(1-x)\right\}, \tag{7.9}$$

where $v^2 + a^2 = 2$.

[5]There could be sizable deviations of the effective WW approximation from the exact result.

The WW cross section receives contributions from several amplitudes, according to the diagrams (a)–(d) [6] in Fig. 9. We have evaluated[7] these contributions and express the result in a form analogous to that of Ref. [4][8]:

$$\begin{aligned}\hat{\sigma}_{WW}(x) &= \frac{G_{\rm F}^2\hat{s}}{64\pi}\beta_h\Bigg\{4\left[\frac{\hat{\mu}_Z\sin(\beta-\alpha)}{1-\hat{\mu}_h}\,\lambda_{hhh}+\frac{\hat{\mu}_Z\cos(\beta-\alpha)}{1-\hat{\mu}_H}\,\lambda_{Hhh}+1\right]^2 g_0 \\ &\quad+\frac{2}{\beta_h}\left[\frac{\hat{\mu}_Z\sin(\beta-\alpha)}{1-\hat{\mu}_h}\,\lambda_{hhh}+\frac{\hat{\mu}_Z\cos(\beta-\alpha)}{1-\hat{\mu}_H}\,\lambda_{Hhh}+1\right] \\ &\qquad\times\left[\sin^2(\beta-\alpha)\,g_1+\cos^2(\beta-\alpha)\,g_2\right] \\ &\quad+\frac{1}{\beta_h^2}\{\sin^4(\beta-\alpha)\,g_3+\cos^4(\beta-\alpha)\,g_4+\sin^2[2(\beta-\alpha)]\,g_5\}\Bigg\}, \qquad (7.10)\end{aligned}$$

where we have introduced 'reduced squared masses'

$$\hat{\mu}_Z = m_Z^2/\hat{s}, \qquad \hat{\mu}_W = m_W^2/\hat{s}, \qquad \hat{\mu}_h = m_h^2/\hat{s}, \qquad \hat{\mu}_H = m_H^2/\hat{s}, \qquad (7.11)$$

and the Higgs velocity is $\beta_h = (1-\hat{\mu}_h)^{1/2}$.

Our approach differs from that of DHZ in that we do not project out the longitudinal degrees of freedom of the intermediate W bosons. Instead, we follow the approach of Ref. [23], where transverse momenta are ignored everywhere except in the W propagators, the integrations over which are approximated as (here p_1 and p_1' denote electron and neutrino momenta, respectively, in the process (7.7)):

$$\int {\rm d}^2\boldsymbol{p}_{1\perp}\,\frac{1}{[(p_1-p_1')^2-m_W^2]^2} \simeq \frac{\pi(1-x_1)}{m_W^2}, \qquad (7.12)$$

where x_1 [and x_2] represents the energy of the W. The energy squared of the subprocess is given as $\hat{s} = (p_1x_1+p_2x_2)^2 = x_1x_2s = xs$.

[6] For each of the diagrams (a) and (d) there are two contributions, corresponding to the interchange of the two Higgs particles.

[7] There are some misprints in Ref. [4], so we present here results of an independent calculation.

[8] In Ref. [4], the factor in front of the term involving g_1 and g_2 reads $\beta_W^2/(\beta_W\beta_h)$; it should be $(1+\beta_W^2)/(\beta_W\beta_h)$. With $\beta_W = 1$, the prefactors in their Eq. (16) reduce to ours.

The contributions of diagrams (b)+(c), (a) and (d) are given by the terms g_0, g_3 and g_4, respectively, with $g_0(x) = 1$, and

$$\begin{aligned} g_3(x) &= 8\beta_h[2\hat{\mu}_W + (\hat{\mu}_h - \hat{\mu}_W)^2][2\hat{\mu}_W + 1 - 3(\hat{\mu}_h - \hat{\mu}_W)^2]\frac{l_W}{a_W} \\ &\quad +16[2\hat{\mu}_W + (\hat{\mu}_h - \hat{\mu}_W)^2]^2 y_W + 16\beta_h^2(1 + a_W)^2, \\ g_4(x) &= 8\beta_h(\hat{\mu}_h - \hat{\mu}_C)^2[1 - 3(\hat{\mu}_h - \hat{\mu}_C)^2]\frac{l_C}{a_C} \\ &\quad +16(\hat{\mu}_h - \hat{\mu}_C)^4 y_C + 16\beta_h^2(1 + a_C)^2, \end{aligned} \tag{7.13}$$

where

$$l_W = \log\frac{1 - 2\hat{\mu}_h + 2\hat{\mu}_W - \beta_h}{1 - 2\hat{\mu}_h + 2\hat{\mu}_W + \beta_h}, \tag{7.14}$$

$$y_W = \frac{2\beta_h^2}{(1 - 2\hat{\mu}_h + 2\hat{\mu}_W)^2 - \beta_h^2}, \tag{7.15}$$

$$a_W = -\tfrac{1}{2} + \hat{\mu}_h - \hat{\mu}_W, \tag{7.16}$$

and similarly l_C, y_C and a_C, with $\hat{\mu}_W$ replaced by $\hat{\mu}_C$, the latter being defined in terms of the charged Higgs mass m_{H^+}.

The interference between diagrams (b)+(c) and (a) is given by the term g_1, whereas the interferences between diagrams (b)+(c) and (d), and between (a) and (d) are given by g_2 and g_5, respectively. For these interference terms, we find

$$\begin{aligned} g_1(x) &= 8[2\hat{\mu}_W + (\hat{\mu}_h - \hat{\mu}_W)^2]l_W - 4\beta_h(1 + 2\hat{\mu}_h - 2\hat{\mu}_W), \\ g_2(x) &= 8(\hat{\mu}_h - \hat{\mu}_C)^2 l_C - 4\beta_h(1 + 2\hat{\mu}_h - 2\hat{\mu}_C), \\ g_5(x) &= \frac{\beta_h}{4}(Z_W l_W + Z_C l_C) + 8\beta_h^2(1 + a_W)(1 + a_C), \end{aligned} \tag{7.17}$$

with

$$Z_W = \frac{(1 + 2a_W)^2}{a_C - a_W}[8\hat{\mu}_W + (1 + 2a_W)^2] + \frac{(1 - 2a_W)^2}{a_C + a_W}[8\hat{\mu}_W + (1 + 2a_W)^2], \tag{7.18}$$

$$Z_C = -\frac{(1 + 2a_C)^2}{a_C - a_W}[8\hat{\mu}_W + (1 + 2a_C)^2] + \frac{(1 + 2a_C)^2}{a_C + a_W}[8\hat{\mu}_W + (1 - 2a_C)^2]. \tag{7.19}$$

Our functions g_1–g_5 correspond to those of DHZ, cf. our Eq. (7.10) and their Eq. (16) in [4]. At small m_h, the cross section is sensitive to small x, where the 'effective WW

approximation' is not well defined, and our results differ from those of DHZ. However, apart from the contributions from small x, our results agree with those of DHZ to a precision of 1–5%.

We show in Fig. 15 the WW fusion cross section, at $\sqrt{s} = 1.5$ TeV, as given by Eqs. (7.1) and (7.8), in the limit of no squark mixing, as well as with mixing (as indicated), and with $\tilde{m} = 1$ TeV. The structure is very reminiscent of that of Fig. 14, and for the same reasons. However, the scale is different.

8 Sensitivity to λ_{Hhh} and λ_{hhh}

Following [4], we have indicated in the m_A–$\tan\beta$ plane the regions where λ_{Hhh} and λ_{hhh} might be measurable, according to criteria analogous to those given there. In Fig. 16, we consider $\sqrt{s} = 500$ GeV, and identify regions according to the following criteria:

(i) Regions where λ_{Hhh} might become measurable are identified as those where $\sigma(H) \times \mathrm{BR}(H \to hh) > 0.1$ fb (solid), with the simultaneous requirement of $0.1 < \mathrm{BR}(H \to hh) < 0.9$ [see Figs. 11–13]. In view of the recent, more optimistic, view on the luminosity that might become available, we also give the corresponding contours for 0.05 fb (dashed) and 0.01 fb (dotted). For $\sigma(H)$ we take the sum of (5.1), (5.2) and (7.1).

(ii) Regions where λ_{hhh} might become measurable are those where the *continuum* $WW \to hh$ cross section [Eq. (7.8)] is larger than 0.1 fb (solid). Also included are contours at 0.05 (dashed) and 0.01 fb (dotted).

Such regions are given for four cases of the mixing parameters A and μ, as indicated. We have excluded from the plots the region where $m_h < 62.5$ GeV, according to the LEP lower bound [10]. This corresponds to low values of m_A.

We note that with an integrated luminosity of 500 fb^{-1}, the contours at 0.1 fb correspond to 50 events per year. This will of course be reduced by efficiencies, but should indicate the order of magnitude that can be reached.

At $\sqrt{s} = 500$ GeV, with a luminosity of 500 fb^{-1} per year, the trilinear coupling λ_{Hhh} is accessible in a considerable part of the m_A–$\tan\beta$ parameter space: at m_A of the order of 200–300 GeV and $\tan\beta$ up to the order of 5. With increasing luminosity, the region extends somewhat to higher values of m_A.

At values of m_A below 100 GeV, there is also a narrow band where λ_{Hhh} is accessible.

The 'steep' edge around $m_A \simeq 200$ GeV (where increased luminosity does not help) is determined by the vanishing of BR($H \to hh$), see Fig. 13.

The coupling λ_{hhh} is accessible in a much larger part of this parameter space, but with a moderate luminosity, 'large' values of $\tan\beta$ are accessible only if A is small.

In Fig. 17, we consider $\sqrt{s} = 1.5$ TeV, and present the analogous contours. Here, for the case of λ_{Hhh} we demand $\sigma(H) \times \mathrm{BR}(H \to hh) > 0.5$ fb (solid) and 0.1 fb (dashed), and for the case of λ_{hhh} we require the corresponding cross section [Eq. (7.8)] to be larger than 0.5 fb (solid) and 0.1 fb (dashed). If a luminosity corresponding to these cross sections becomes available at $\sqrt{s} = 1.5$ TeV, a somewhat larger region than at $\sqrt{s} = 500$ GeV is accessible in the m_A–$\tan\beta$ plane.

It should be stressed that the requirements discussed here are necessary, but not sufficient conditions for the trilinear couplings to be measurable. We also note that there might be sizable corrections to the WW approximation, and that it would be desirable to incorporate the dominant two-loop corrections to the trilinear couplings in the calculations.

9 Conclusions

We have carried out a detailed investigation of the possibility of measuring the MSSM trilinear couplings λ_{Hhh} and λ_{hhh} at an e^+e^- collider. Where there is an overlap, we have confirmed the results of Ref. [4]. Our emphasis has been on taking into account all the parameters of the MSSM Higgs sector. We have studied the importance of mixing in the squark sector, as induced by the trilinear coupling A and the bilinear coupling μ.

At moderate energies ($\sqrt{s} = 500$ GeV) the range in the m_A–$\tan\beta$ plane that is accessi-

ble for studying λ_{Hhh} changes quantitatively for non-zero values of the parameters A and μ. As far as the coupling λ_{hhh} is concerned, however, there is a qualitative change from the case of no mixing in the squark sector. If A is large, then high luminosity is required to reach 'high' values of $\tan\beta$. At higher energies ($\sqrt{s} = 1.5$ TeV), the mixing parameters A and μ change the accessible region of the parameter space only in a quantitative manner.

Acknowledgements

P. O. would like to thank the DESY Theory Group and the CERN Theory Division, whereas P. N. P. would like to thank the University of Bergen, for kind hospitality while parts of this work were finished. It is also a pleasure to thank Abdel Djouadi, Wolfgang Hollik, Bernd Kniehl, Conrad Newton and Peter Zerwas for valuable discussions and advice. This research was supported by the Research Council of Norway, and (PNP) by the University Grants Commission, India under project number 10-26/98(SR-I).

References

[1] J. F. Gunion, H. E. Haber, G. Kane and S. Dawson, *The Higgs Hunter's Guide*, Addison-Wesley, New York, 1990.

[2] For reviews, see H.-P. Nilles, Phys. Rep. **110**, 1 (1984); H. E. Haber and G. L. Kane, Phys. Rep. **C117**, 75 (1985); R. Barbieri, Riv. Nuovo Cimento **11** No. 4, p. 1 (1988).

[3] T. Plehn, M. Spira and P. M. Zerwas, Nucl. Phys. **B479**, 46 (1996).

[4] A. Djouadi, H. E. Haber and P. M. Zerwas, Phys. Lett. **B375**, 203 (1996) and Erratum, to be published.

[5] See, e.g., ECFA/DESY LC Physics Working Group (E. Accomando et al.), Phys. Rep. **299**, 1 (1998). The luminosity quoted there is now believed to be too conservative.

[6] J. Ellis, G. Ridolfi and F. Zwirner, Phys. Lett. **B257**, 83 (1991); Y. Okada, M. Yamaguchi and T. Yanagida, Prog. Theor. Phys. **85**, 1 (1991); H. E. Haber and R. Hempfling, Phys. Rev. Lett. **66**, 1815 (1991).

[7] J. Ellis, G. Ridolfi and F. Zwirner, Phys. Lett. **B262**, 477 (1991).

[8] R. Hempfling and A. H. Hoang, Phys. Lett. **B331**, 99 (1994);
M. Carena, J.R. Espinosa, M. Quirós and C.E.M. Wagner, Phys. Lett. **B355**, 209 (1995);
M. Carena, M. Quirós and C.E.M. Wagner, Nucl. Phys. **B461**, 407 (1996);
S. Heinemeyer, W. Hollik and G. Weiglein, Phys. Rev. **D58**, 091701 (1998).

[9] B. Kileng, P. Osland and P. N. Pandita, Z. Phys. **C71**, 87 (1996); B. Kileng, P. Osland and P. N. Pandita, in *Xth International Workshop: High Energy Physics and Quantum Field Theory*, Proceedings of the conference, Zvenigorod, Russia, 1995, ed. B.B. Levtchenko and V.I. Savrin (Moscow University Press, Moscow,

1996), p. 167 (hep-ph/9601284); B. Kileng, P. Osland and P. N. Pandita, in Proceedings of the International Workshop on *Quantum Systems: New Trends and Methods*, Minsk, Belarus, 1996, eds. Y. S. Kim, L. M. Tomil'chik, I. D. Feranchuk and A. Z. Gazizov (World Scientific, Singapore, 1997), p. 231 (hep-ph/9608315).

[10] R. Barate *et al.* (ALEPH Collaboration), Phys. Lett. **B412**, 173 (1997).

[11] R. Barate *et al.* (ALEPH Collaboration), CERN-EP-98-145, Sep 1998.

[12] M. Carena, P. H. Chankowski, S. Pokorski and C. E. M. Wagner, CERN-TH/98-148, hep-ph/9805349.

[13] V. Barger, M. S. Berger, A. L. Stange and R. J. N. Phillips, Phys. Rev. **D45**, 4128 (1992).

[14] A. Sirlin and R. Zucchini, Nucl. Phys. **B266**, 389 (1986).

[15] A. Djouadi, J. Kalinowski and P. M. Zerwas, Z. Phys. **C70**, 435 (1996).

[16] G. Pócsik and G. Zsigmond, Z. Phys. **C10**, 367 (1981).

[17] J. F. Gunion, L. Roszkowski, A. Turski, H. E. Haber, G. Gamberini, B. Kayser, S. F. Novaes, F. Olness and J. Wudka, Phys. Rev. **D38**, 3444 (1988).

[18] H. E. Haber, in Proceedings of the Conference on *Perspectives for Electroweak Interactions in* e^+ e^- *Collisions*, Ringberg (Tegernsee), Germany, 1995; ed. B. A. Kniehl (World Scientific, Singapore, 1995) p. 219.

[19] For recent references, see: A. Djouadi, P. Janot, J. Kalinowski, P.M. Zerwas, Phys. Lett. **B376**, 220 (1996);
A. Bartl, H. Eberl, K. Hidaka, T. Kon, W. Majerotto and Y. Yamada, hep-ph/9709253, in *Beyond the Standard Model, 5th International Conference on Physics Beyond the Standard Model*, Balholm, Norway, eds. G. Eigen, P. Osland and B. Stugu (AIP, Woodbury, N.Y., 1997), p. 494.

[20] A. Djouadi, J. Kalinowski and P. M. Zerwas, in Proceedings, Workshop on e^+e^- *Collisions at 500 GeV: The Physics Potential*, Munich-Annecy-Hamburg (DESY 92-123 A, Hamburg, 1992).

[21] A. Djouadi, D. Haidt, B. A. Kniehl, B. Mele and P. M. Zerwas, ibid.

[22] R. N. Cahn and S. Dawson, Phys. Lett. **B136**, 196 (1984); S. Dawson, Nucl. Phys. **B249**, 42 (1984); M. Chanowitz and M. K. Gaillard, Phys. Lett. **B142**, 85 (1984); I. Kuss and H. Spiesberger, Phys. Rev. **D53**, 6078 (1996).

[23] G. Altarelli, B. Mele and F. Pitolli, Nucl. Phys. **B287**, 205 (1987).

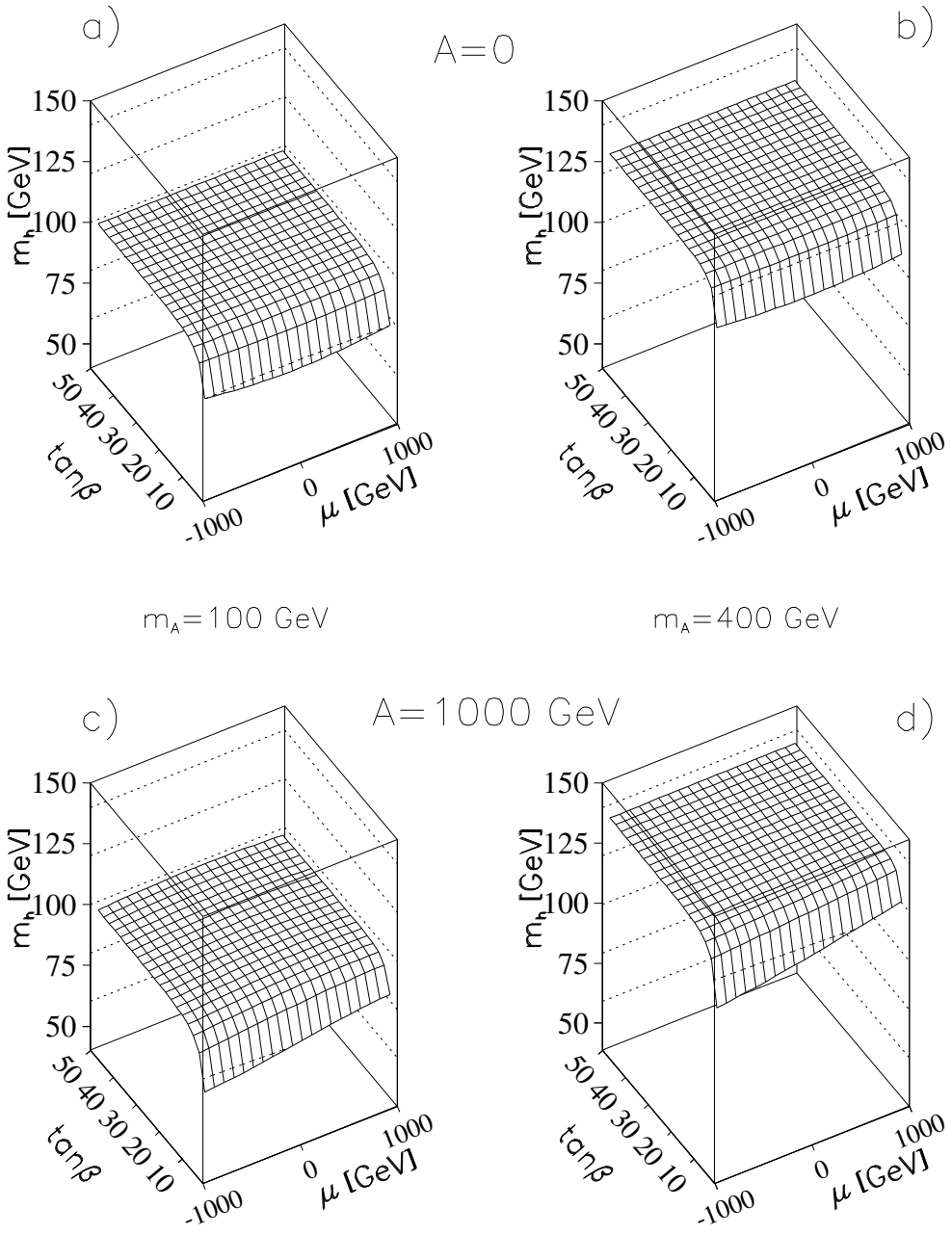

Figure 1: Mass of the lightest Higgs boson m_h as a function of μ and $\tan\beta$. Two values of m_A and two values of A are considered: a) $m_A = 100$ GeV, $A = 0$, b) $m_A = 400$ GeV, $A = 0$ GeV, c) $m_A = 100$ GeV, $A = 1$ TeV, d) $m_A = 400$ GeV, $A = 1$ TeV. We have taken $\tilde{m} = 1$ TeV.

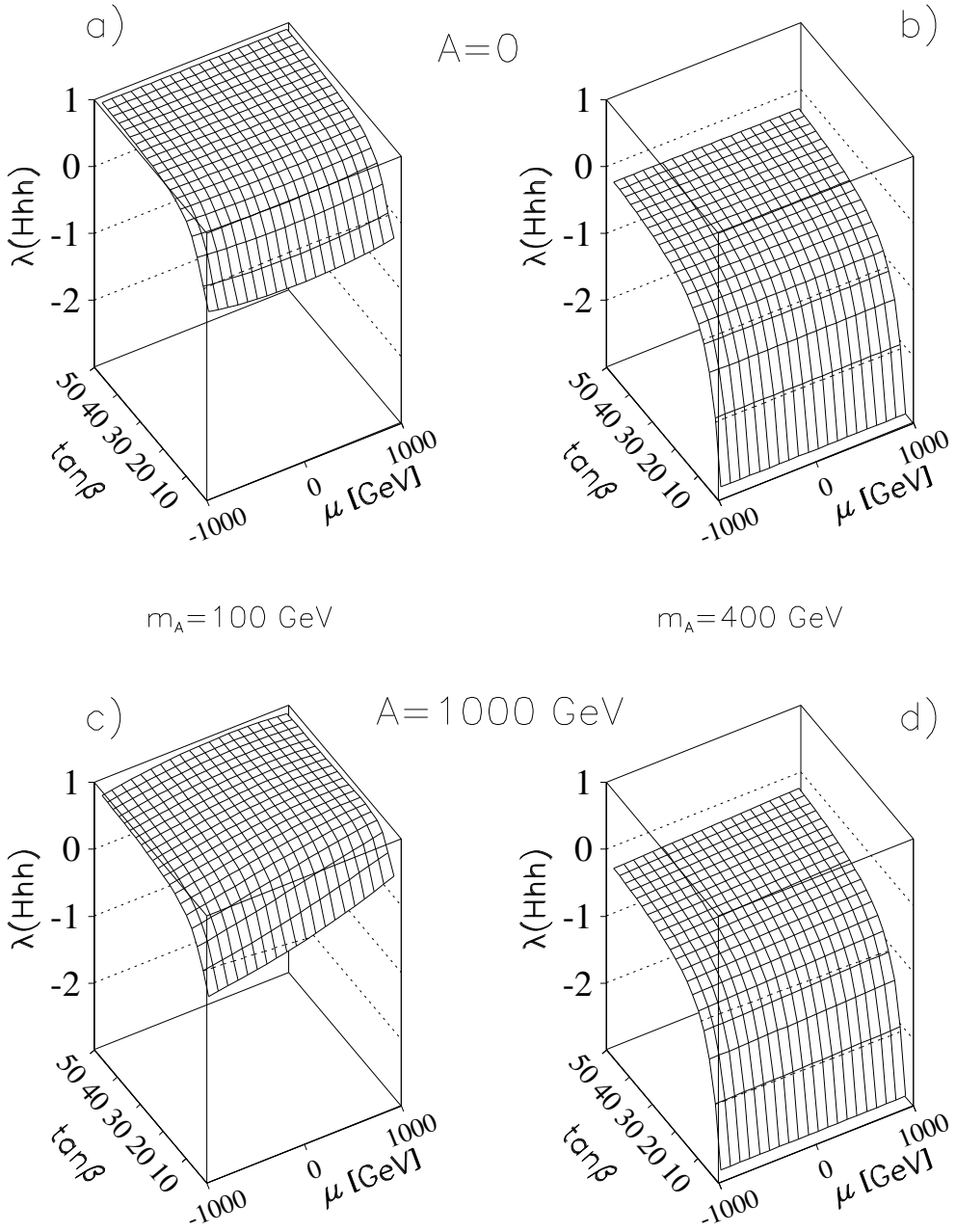

Figure 2: Trilinear Higgs coupling λ_{Hhh} as a function of μ and $\tan\beta$. The values of the parameters are the same as in Fig. 1.

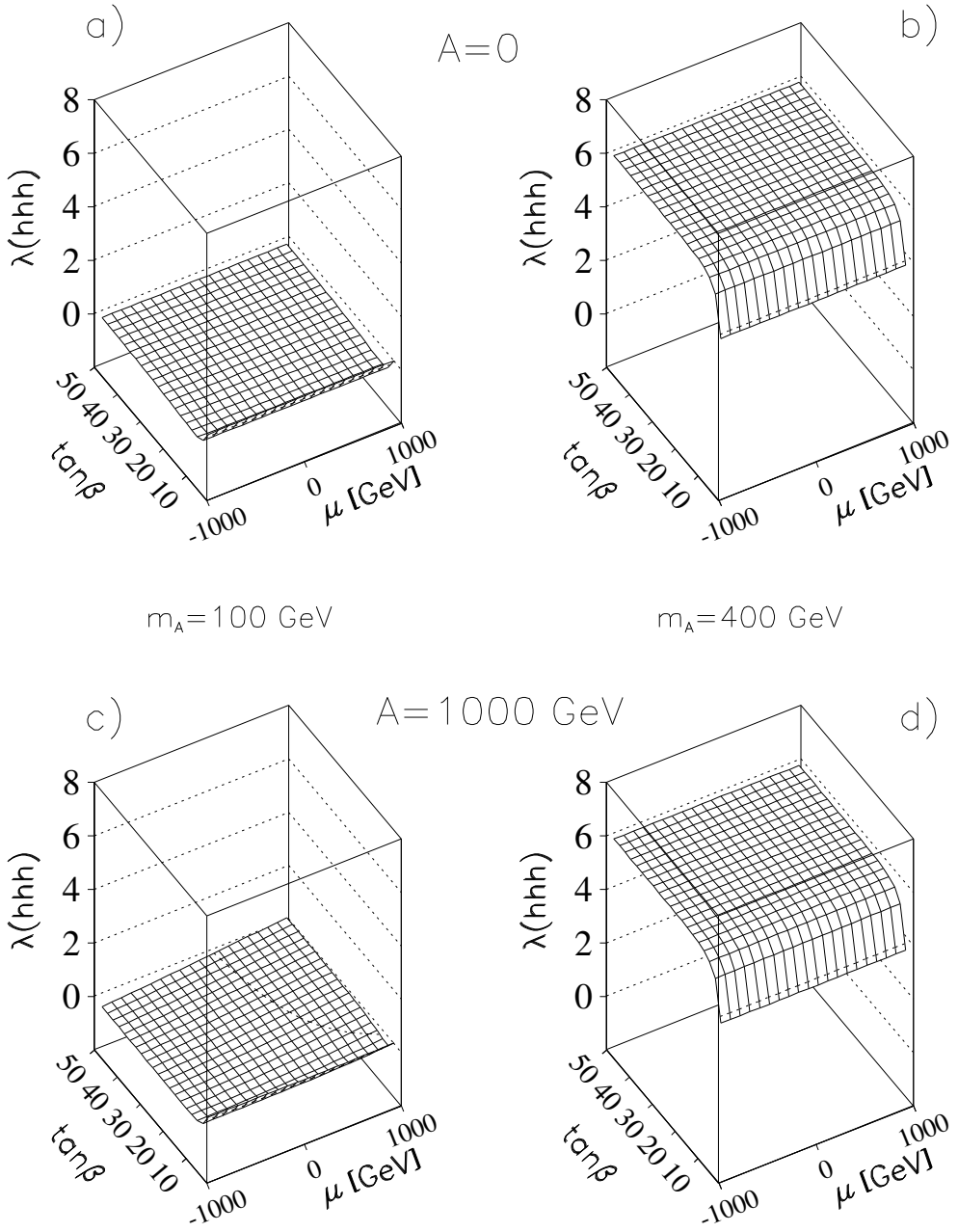

Figure 3: Trilinear Higgs coupling λ_{hhh} as a function of μ and $\tan\beta$. The values of the parameters are the same as in Fig. 1.

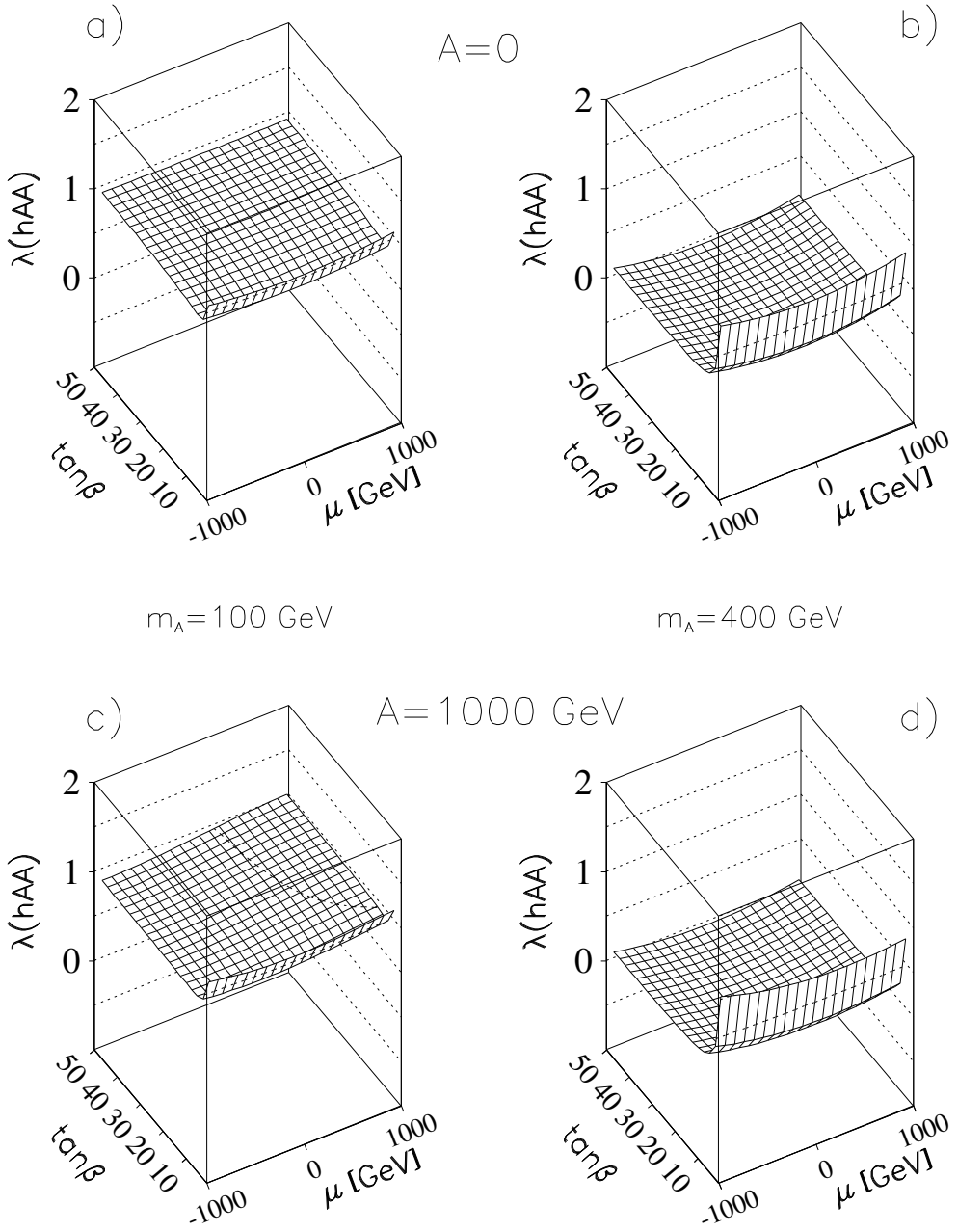

Figure 4: Trilinear Higgs coupling λ_{hAA} as a function of μ and $\tan\beta$. The values of the parameters are the same as in Fig. 1.

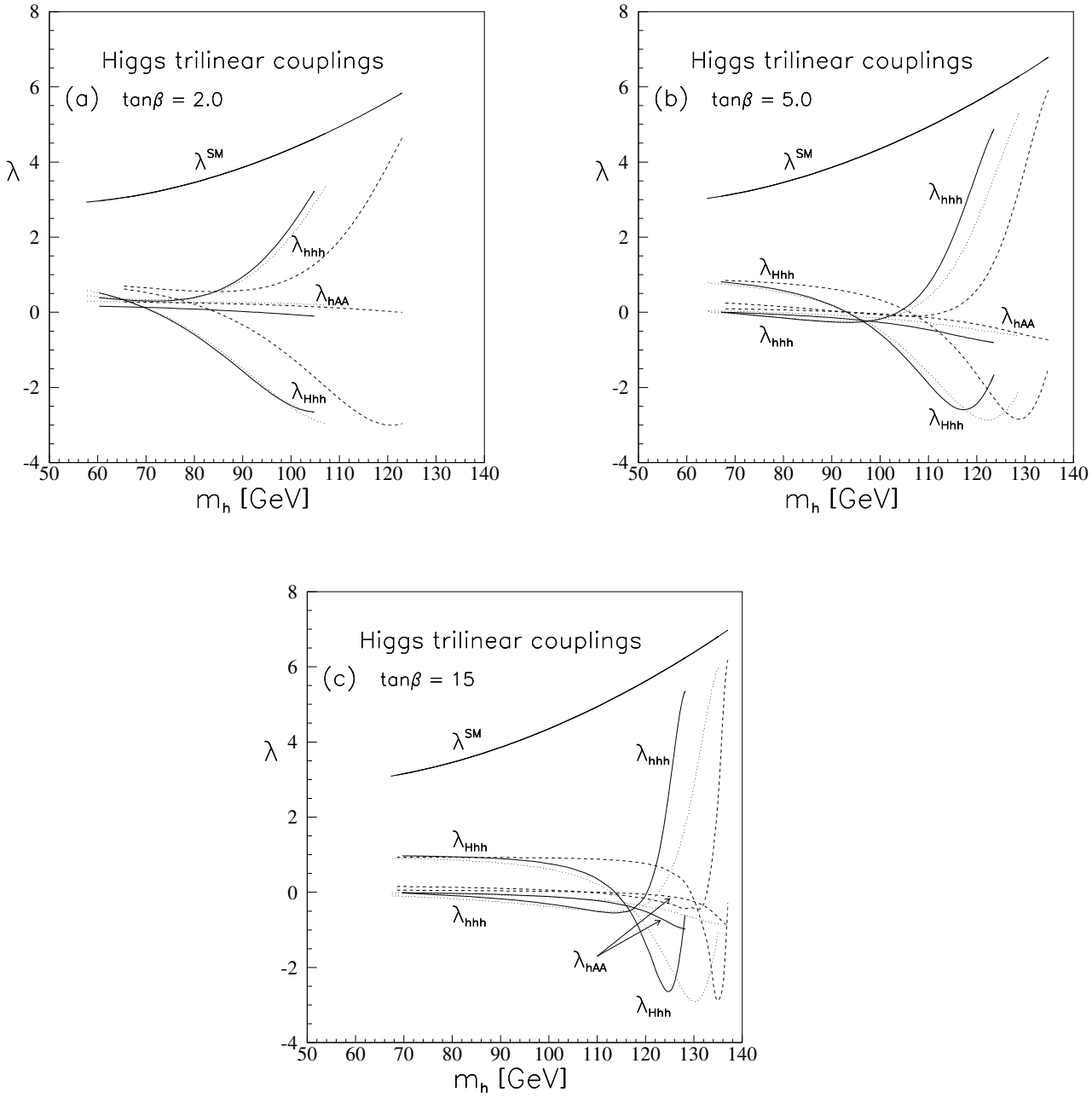

Figure 5: Trilinear Higgs couplings λ_{Hhh}, λ_{hhh} and λ_{hAA} as functions of m_h for three values of $\tan\beta$: (a) $\tan\beta = 2.0$, (b) $\tan\beta = 5.0$, (c) $\tan\beta = 15$. Each coupling is shown for three cases of the mixing parameters: no mixing ($A = 0$, $\mu = 0$, solid), mixing with $A = 1$ TeV and $\mu = -1$ TeV (dotted), as well as $A = 1$ TeV and $\mu = 1$ TeV (dashed). For comparison the SM quartic coupling $\lambda^{\rm SM}$ is also shown.

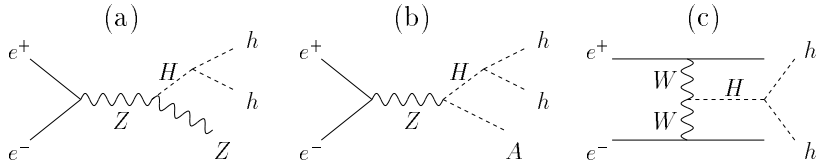

Figure 6: Feynman diagrams for the resonant production of hh final states in e^+e^- collisions. Diagrams (a) and (b) represent the production of H in association with Z and A, respectively, whereas diagram (c) is the WW fusion mechanism for the production of H. The Higgs boson H decays via $H \to hh$ to produce the two-Higgs final state.

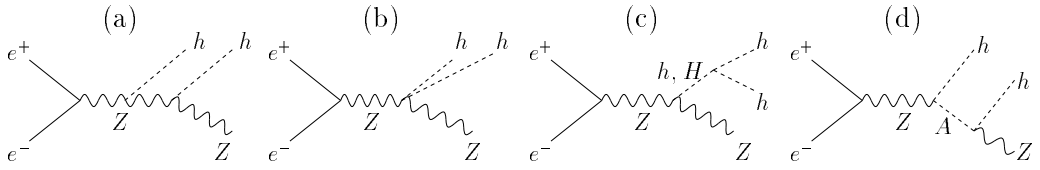

Figure 7: Feynman diagrams for the non-resonant production of hh final states in association with Z. The diagram (d), with A produced on the mass shell, which subsequently decays via $A \to hZ$, is a background to the resonance process, Fig. 6a.

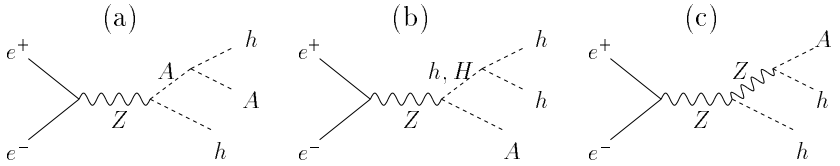

Figure 8: Feynman diagrams for the associated production of hh with the pseudoscalar A in the continuum.

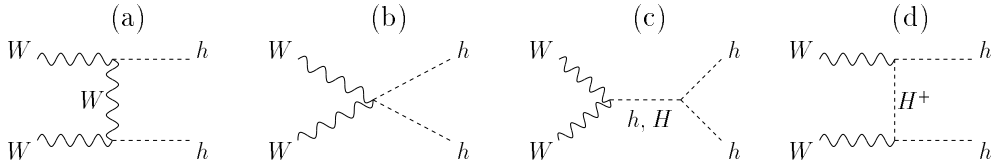

Figure 9: Feynman diagrams for the non-resonant WW fusion mechanism for the production of hh states in e^+e^- collisions.

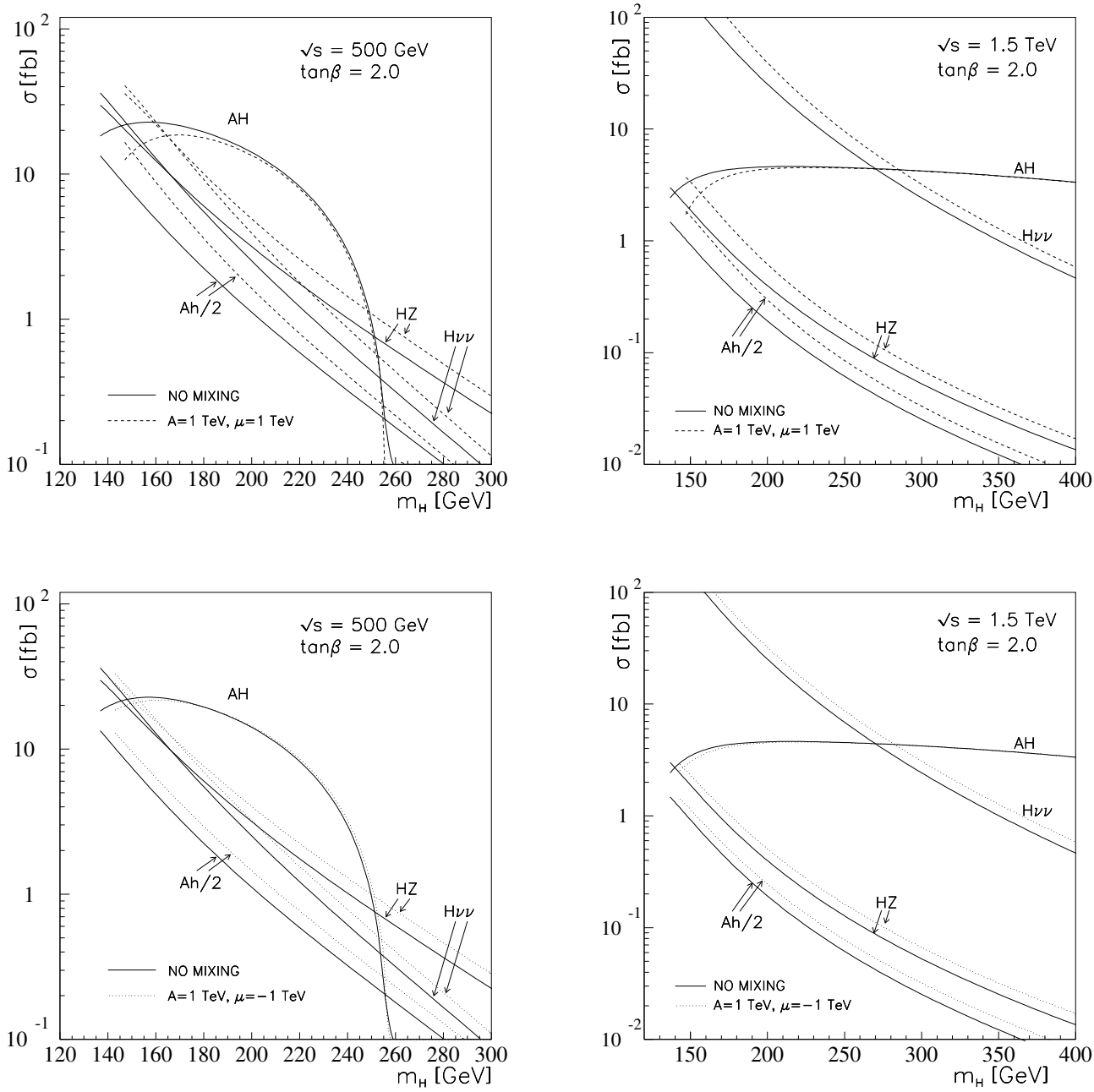

Figure 10: Cross sections for the production of the heavy Higgs boson H in e^+e^- collisions. Also shown is the cross section for the background process in which Ah is produced in the final state. We have taken $\sqrt{s} = 500$ GeV and 1.5 TeV. Solid curves are for no mixing, $A = 0$, $\mu = 0$. Dashed and dotted curves refer to mixing: $A = 1.0$ TeV, $\mu = 1.0$ TeV (dashed) and $A = 1.0$ TeV, $\mu = -1.0$ TeV (dotted).

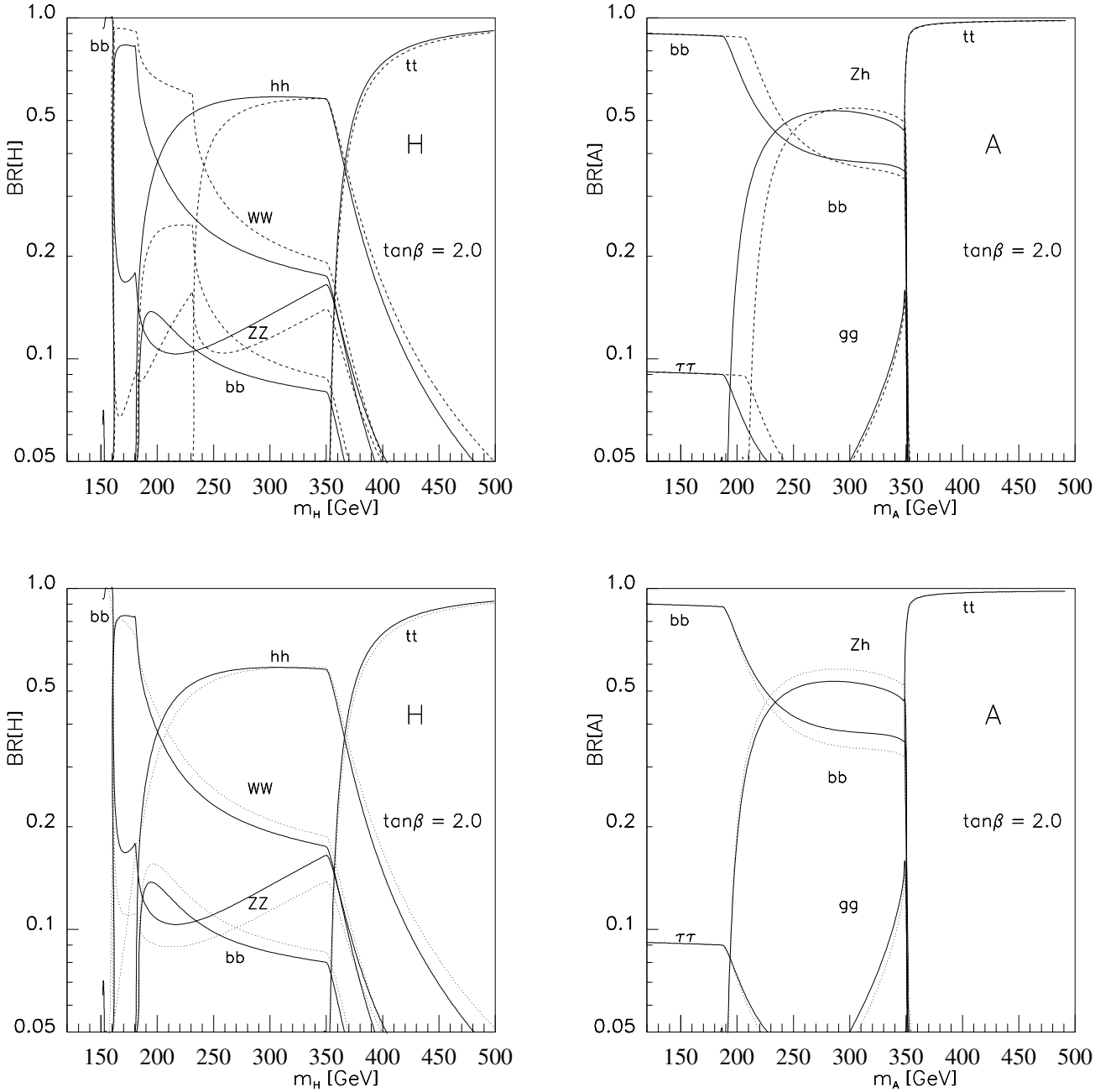

Figure 11: Branching ratios for the decay modes of the CP-even heavy Higgs boson H, and the CP-odd Higgs boson A for $\tan\beta = 2.0$. Solid curves are for no mixing, $A = 0$, $\mu = 0$. Dashed and dotted curves refer to mixing: $A = 1.0$ TeV, $\mu = 1.0$ TeV (dashed) and $A = 1.0$ TeV, $\mu = -1.0$ TeV (dotted).

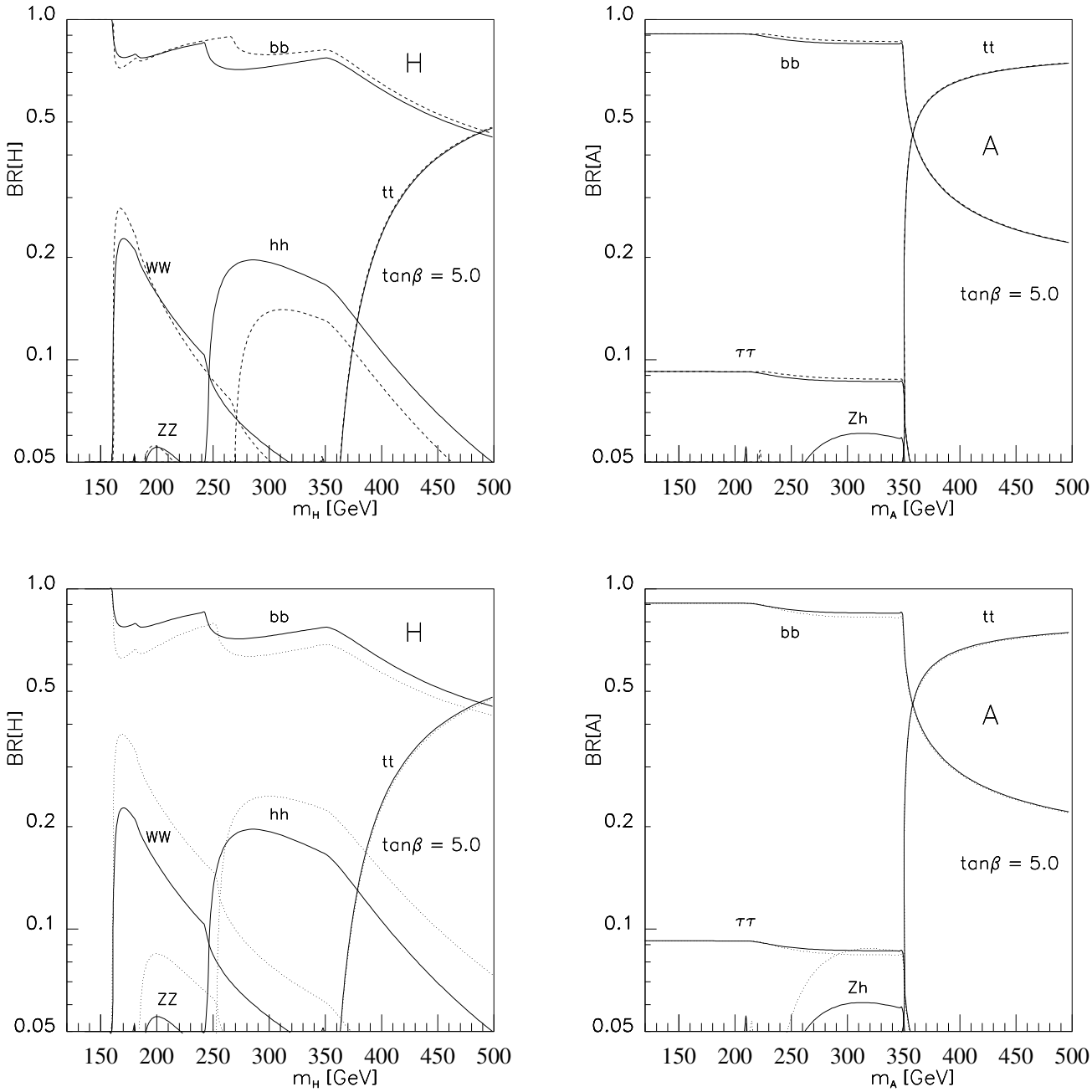

Figure 12: As in Fig. 11, but with $\tan\beta = 5.0$. Solid curves are for no mixing, $A = 0$, $\mu = 0$. Dashed and dotted curves refer to mixing: $A = 1.0$ TeV, $\mu = 1.0$ TeV (dashed) and $A = 1.0$ TeV, $\mu = -1.0$ TeV (dotted).

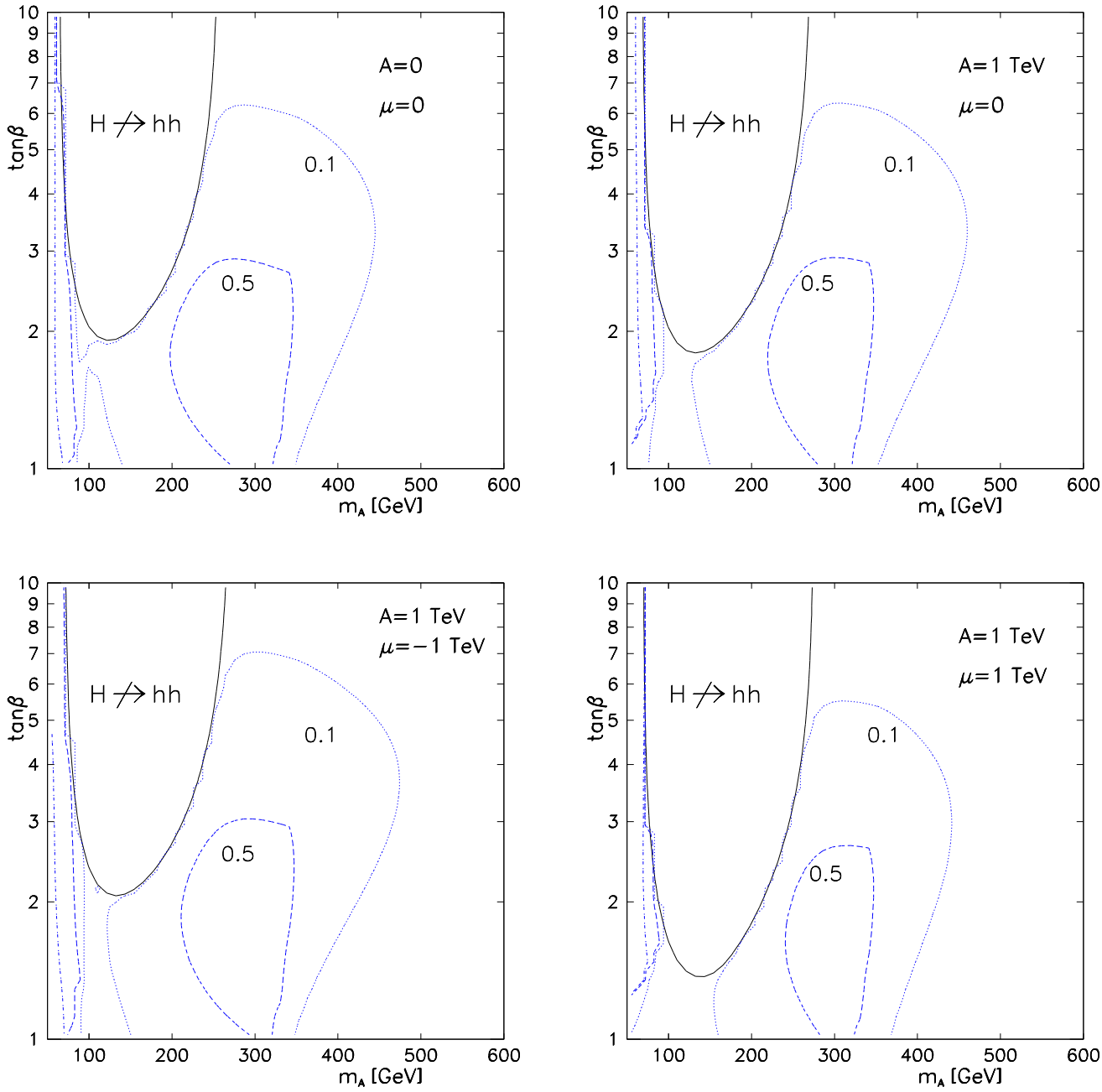

Figure 13: The region in the m_A–$\tan\beta$ plane where the decay $H \to hh$ is kinematically *forbidden* is indicated by a solid line contour. Also given are contours at which the branching ratio equals 0.1 (dotted), 0.5 (dashed) and 0.9 (dash-dotted, at the far left). Four cases of mixing parameters A and μ are considered, as indicated.

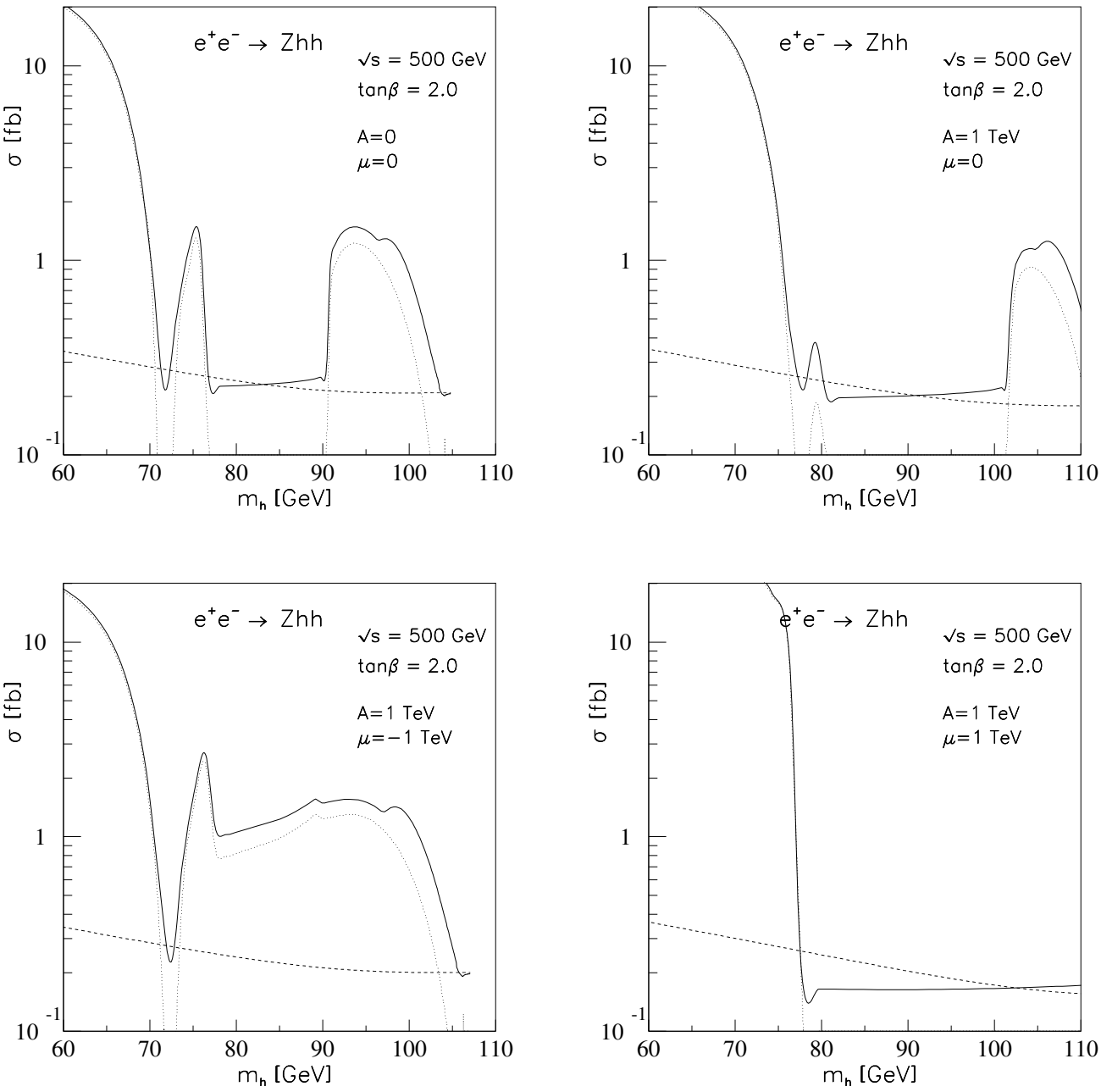

Figure 14: Cross section $\sigma(e^+e^- \to Zhh)$ as a function of m_h, for four cases: (a) no mixing, (b)–(d) $A = 1$ TeV, $\mu = 0$, -1 and 1 TeV, as indicated. The dotted curve is the resonant production. The dashed curve gives the decoupling limit.

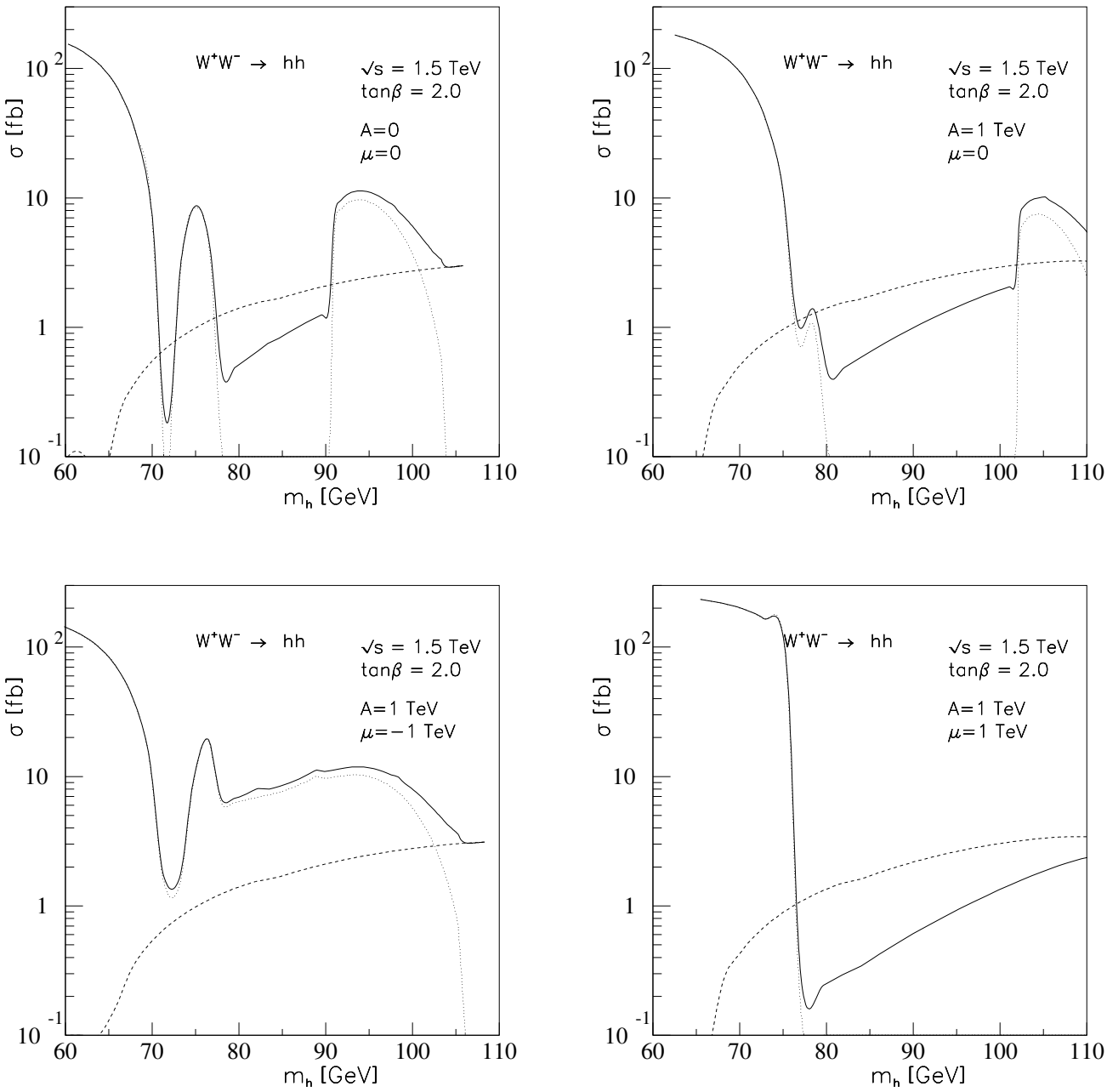

Figure 15: Cross section $\sigma(e^+e^- \to \nu_e\bar{\nu}_e hh)$ (via WW fusion) as a function of m_h, for four cases: (a) no mixing, (b)–(d) $A = 1$ TeV, $\mu = 0$, -1 and 1 TeV, as indicated. The dotted curve is the resonant production. The dashed curve gives the decoupling limit.

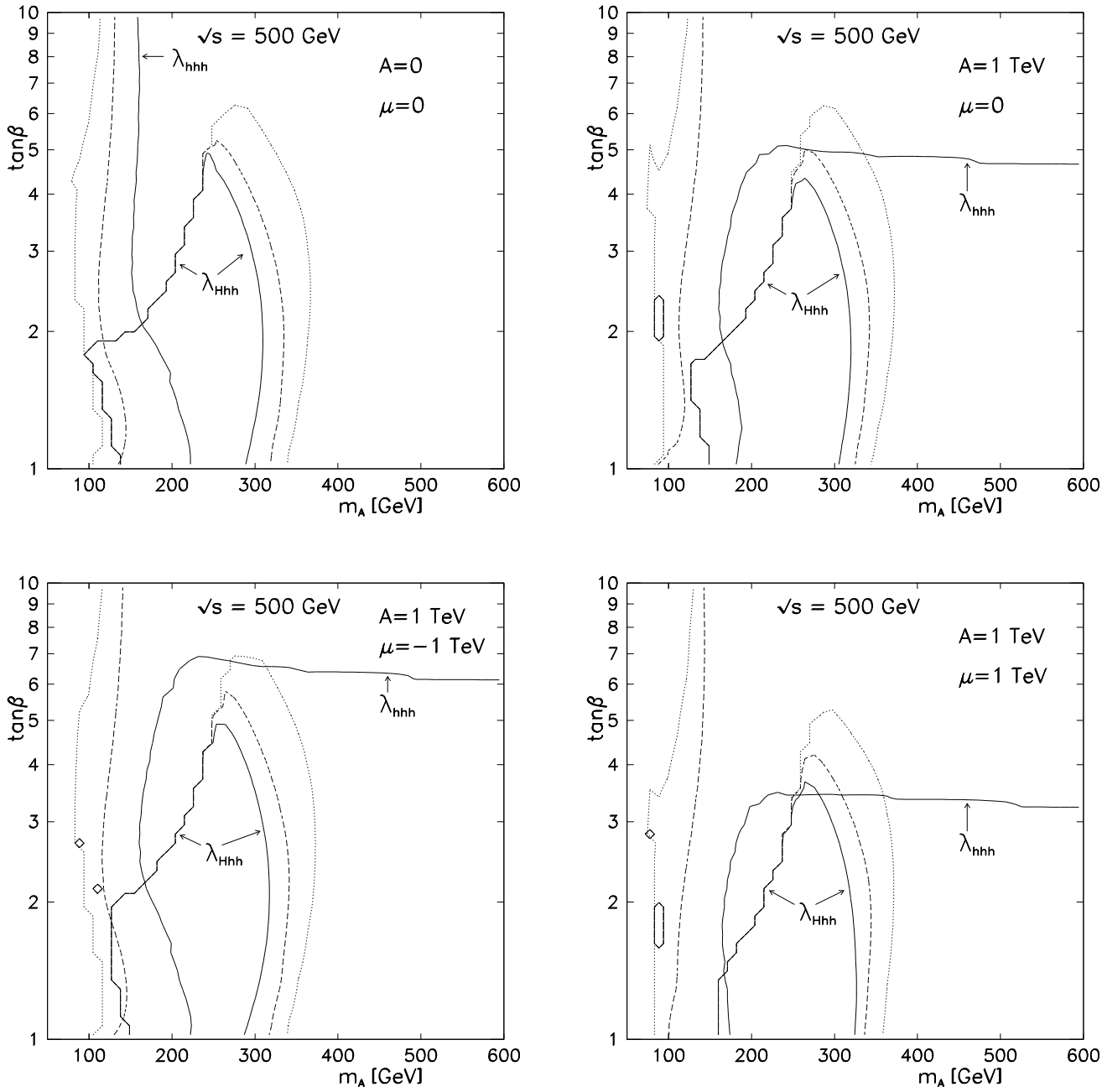

Figure 16: Regions where trilinear couplings λ_{Hhh} and λ_{hhh} might be measurable at $\sqrt{s} = 500$ GeV. Inside contours labelled λ_{Hhh}, $\sigma(H) \times$ BR$(H \to hh) > 0.1$ fb (solid), while $0.1 <$ BR$(H \to hh) < 0.9$. Inside (to the right or below) contour labelled λ_{hhh}, the *continuum* $WW \to hh$ cross section exceeds 0.1 fb (solid). Analogous contours are given for 0.05 (dashed) and 0.01 fb (dotted). Four cases of mixing are considered, with $A = 0$ or 1 TeV, and $\mu = 0$ or ± 1 TeV, as indicated.

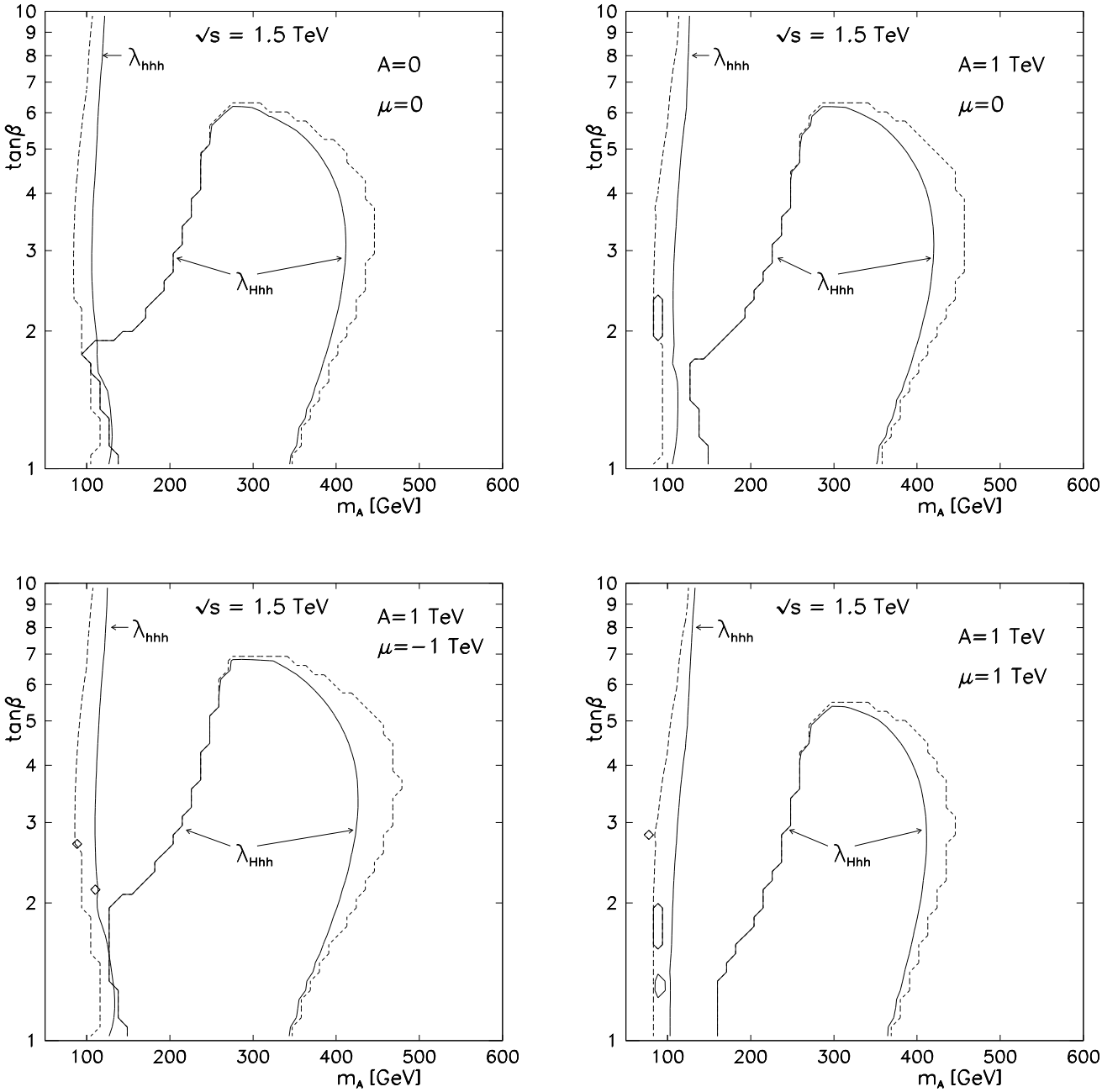

Figure 17: Regions where trilinear couplings λ_{Hhh} and λ_{hhh} might be measurable at $\sqrt{s} = 1.5$ TeV. The contours correspond to 0.5 fb (solid) and 0.1 fb (dashed). All other parameters are the same as in Fig. 16.